CHARACTERIZATION OF A STRUCTURE CONSISTING OF MAGNETOSTATIC RESPONSIVE MICROSCOPIC PARTICLES AND ITS APPLICATION IN ANTENNAS

A Dissertation
Submitted to the Graduate Faculty
of the
North Dakota State University
of Agriculture and Applied Science

By

Adnan Iftikhar

In Partial Fulfillment of the Requirements
for the Degree of
DOCTOR OF PHILOSOPHY

Major Department:
Electrical and Computer Engineering

November 2015

Fargo, North Dakota

NORTH DAKOTA STATE UNIVERSITY

Graduate School

Title

Characterization of a Structure Consisting of Magnetostatic Responsive Microscopic Particles and Its Application In Antennas

By

Adnan Iftikhar

The supervisory committee certifies that this ***disquisition*** complies with North Dakota State University's regulations and meets the accepted standards for the degree of

DOCTOR OF PHILOSOPHY

SUPERVISORY COMMITTEE:

Dr. Benjamin D. Braaten
Chair

Dr. David A. Rogers

Dr. Ivan T. Lima Jr.

Dr. Yechun Wang

Approved:

Nov. 20, 2015
Date

Scott C. Smith
Department Chair

ABSTRACT

Wireless communication systems often require that a single antenna work at different frequencies. Thus the reconfigurable antennas are useful in frequency agile environments to receive a signal over multiple bands. Research on antenna reconfigurability using mechanical systems and radio frequency (RF) switches have been implemented in the past years. One problem for these voltage-controlled switches is that they require direct current (DC) bias control lines for operation. The incorporation of DC biasing circuitry also limits designers to explore the reconfigurable capacity of many antennas. The DC bias control lines can possibly degrade the antenna performance. Moreover, because of the additional control signals, many existing multiband systems cannot use reconfigurable antennas. In this research, magnetostatic responsive particles are used in micro-sized cavities to manufacture novel magnetic switches that are activated in a magnetic field. Furthermore, the characterization, modeling in simulation software, and lumped element model extraction of these micro electromechanical systems (MEMS) based on magnetic switches is presented. A refined method of quantifying the micro sized magnetic particles in a cavity and the response of the proposed micro level magnetic switches in the RF field is also explained in detail. Then, a microstrip patch antenna loaded with Electromagnetic Band Gaps (EBGs) that cannot be reconfigured using existing RF switching devices was reconfigured using the proposed magnetic switches and is presented in this research for the first time. A comparison between PIN diodes and the proposed magnetic switches on a microstrip patch is also included in this research to show the efficiency of the proposed structure. Overall, the proposed magnetic switches showed good results when used in antenna systems to achieve reconfigurability and do not effect the radiation characteristics of the reconfigured antenna.

ACKNOWLEDGMENTS

I am sincerely grateful to my advisor, Dr. Benjamin D. Braaten, for his thorough support, guidance and innovative ideas throughout my PhD studies. I would also like to offer my sincere and deep hearted gratitude to my advisor who always encouraged me and persistently conveyed the spirit and guidance required for the research. Without his kind guidance and continuous efforts, this disquisition would not have been possible. He is a thorough gentleman who leads the way. Not only did he inculcated the academic knowledge but also presented the moral and ethical examples to follow.

Also I would like to express appreciation to my committee members, Dr. David A. Rogers, Dr. Ivan T. Lima Jr., and Dr. Yechun Wang for their support, guidance, and helpful recommendations. A special thanks to Electrical and Computer Engineering staff members Jeffrey Erickson (Engineering Technician), Laura D. Dallman, and Priscilla Schlenker for all the unconditional help and favors.

Most importantly, none of this would have been possible without the continuous support, motivation, love, and patience of my parents and my wife. I especially like to pray and remember my great grand father (late) who is the only and every reason for whatever I am today and whatever I achieved in my life. I would also like to thank my loving brothers and sister for their love and support.

Finally, I owe my heartiest thanks to COMSATS Institute of Information Technology, Pakistan for granting me the PhD. scholarship and to my advisor for the financial support from various fundings during my PhD. studies.

DEDICATION

I would like to dedicate this thesis to my parents, brothers, sister, and to my wife.

TABLE OF CONTENTS

LIST OF FIGURES

LIST OF SYMBOLS

f ..... Frequency

λ ..... Wavelength

ϵ ..... Permittivity

ϵ_r ..... Relative permeability

$\tan\delta$ ..... Loss tangent

h ..... Cavity depth/substrate thickness

d ..... Cavity diameter of the magnetic switch

V ..... Volume of the cyliderical cavity

K ..... Volume of the cyliderical cavity

η ..... Density of spherical particles

N ..... Number of magnetic particles

N_T ..... Total number of magnetic particles

N_s ..... Minimum number of particles per column

L_{tape} ..... Inductance due to the copper tape

C_{gap} ..... Gap capacitance

C_f ..... Fringing capacitance

C_{cavity} ..... Cavity capacitance

C_p ..... Open end fringing capacitance of the copper tape

$R_{particle}$ ..... Resistance of the particles

$L_{particle}$ ..... Inductance of the magnetic particles

C_{switch} ..... Magnetic switch substrate capacitance

$C_{tape,air}$ ..... Capacitance between air and copper tape

$C_{tape,diel}$ ..... Capacitance between host substrate and copper tape

CHAPTER 1. AN INTRODUCTION TO RECONFGURABLE ANTENNAS AND PROPOSED RESEARCH

Multi-functionality in antenna systems has been a topic of great interest for researchers from the past three decades [1]. Multi-functionality options to provide liberty to the users to connect with different kinds of services for various applications-oriented tasks at different times. To accomplish this it is desirable to design single radiating elements having multifunction capabilities [2], such as reconfigurable antenna systems. Software defined radios, MIMO systems, cognitive radio, and phased arrays are the potential examples of reconfigurable antennas. In antenna systems, reconfigurability is achieved by using phase shifters, tuneable elements in the feeding network, mechanical means, Radio Frequency Micro-Electro-Mechanical Systems (RF MEMS), Field Effect Transistors (FETs), and PIN diodes. These existing technologies that are used to reconfigure the antenna system require DC power and biasing circuitry for their operation and because of the flow of the RF current, antenna efficiency can be degraded due to losses. This required biasing circuitry also limits some of the antennas to be reconfigured using existing technologies.

1.1. Statement of the Topic

The idea of a magnetic switch to obtain the reconfigurability is being proposed for the first time in this work. An external magnetic field will be used to excite the magnetic switch which will eliminate the requirement of the biasing circuitry on the antenna system. This research will first focus on the initial manufacturing of the magnetic switch, packaging of the magnetic switch, its behavior in the RF field, and its applications in the RF switching and antenna reconfigurability.

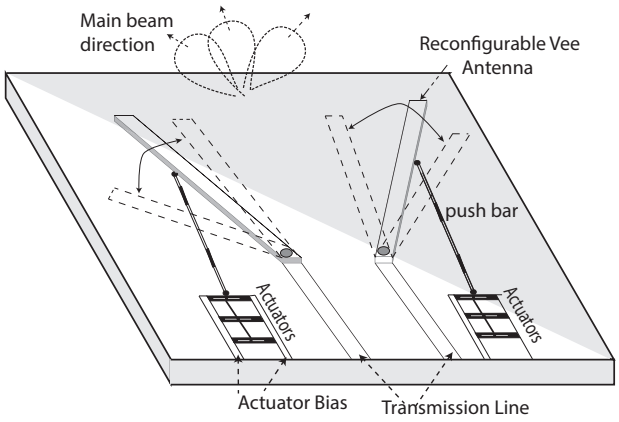

Figure 1. Isometric view of scratch drive actuated 17.5 GHz Vee Antenna [6].

1.2. Contributions

The contributions of this research are, manufacturing magnetic switches, characterization of the magnetic switch, a compact antenna with reconfigurable characteristics in frequency of operation that cannot be reconfigured using PIN diodes and existing technologies. Furthermore, this research will provide a comparison between the magnetic switch and the PIN diode by reconfiguring an antenna using the proposed magnetic switch and the PIN diodes.

1.3. Previous Work on Reconfigurable Antennas

Reconfigurable antennas have been around since the 1930s. Initially, they were based on mechanical movement of a feed or antenna part [3] - [4]. Antenna arrays took reconfigurability to a new level with electronic control of the antenna's pattern. MEMS and semiconductor switches have been at the heart of most reconfigurable antenna research since the late 1990s. MEMS switches are tiny mechanical switches packaged on a substrate (silicon, quartz, and glass). Antenna reconfigurability using a MEMS switch is reported in [5] - [9].

Figure 1 shows an illustration of the antenna in which each radiating arm has independent movement that in return gives the possibility of beam shaping and far-

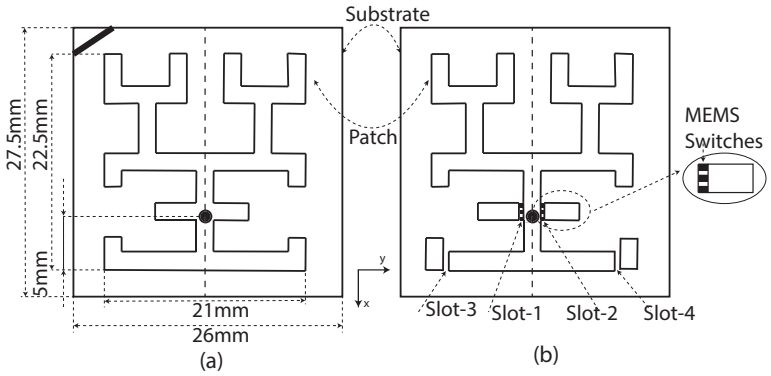

Figure 2. (a) Original antenna layout. (b) Antenna configuration with the MEMS switches [10].

field beam steering. The work in [10] demonstrates the use of the MEMS Switch incorporated in a 3rd order Hilbert curve fractal antenna.

The use of a MEMS switch reconfigures the resonant frequency from 10 GHz to 12 GHz and the structural loading of the antenna is shown in Figure 2. The single arm square antenna's reconfigurability is achieved in [11]- [14] in terms of radiation and frequency using RF MEMS switches. The outer edge of the arm is shorted to the ground and two RF switches are used for reconfigurability by changing the electrical length of the radiating element. The RF chokes are used to reduce the insertion loss

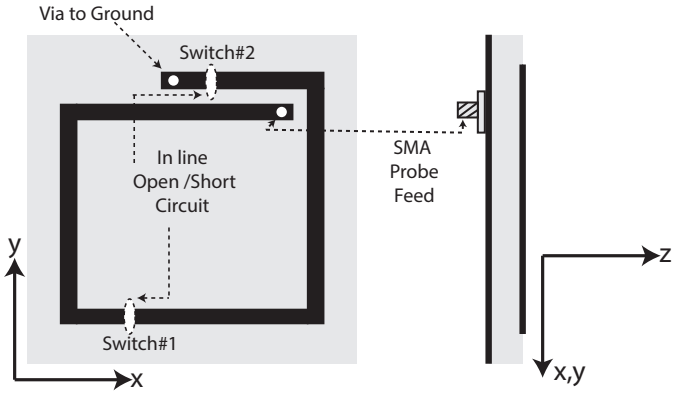

Figure 3. Single arm square antenna configuration [11].

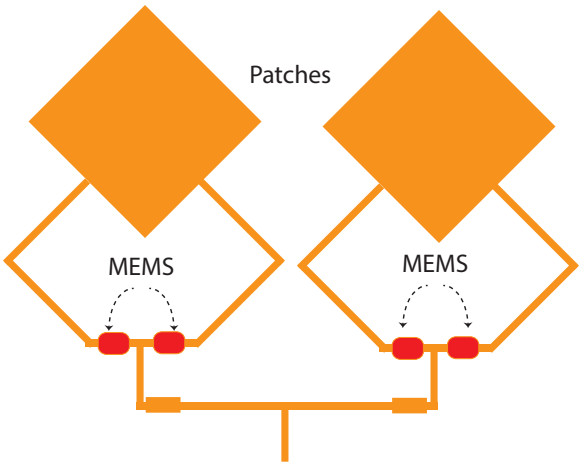

Figure 4. A reconfigurable antenna that changes polarization using MEMS [15].

that results from biasing the path connected to the RF part in the PIN diode switches as shown in Figure 3.

Reconfigurable antennas can also change the antenna's polarization. As depicted in Figure 4, placing the MEMS switches in the feeds of micro-strip antenna [15] provides the ability to switch from linear polarization to the orthogonal linear polarization, or to circular polarization.

Semiconductor RF switches such as PIN diodes and FETs have also been used to re-configure antennas. The work in [16] presents a microstrip patch antenna for polarization reconfigurability. The radiating elements are incorporated with two orthogonal slots and the diodes are used for establishing the 'ON' or 'OFF' connection between the slots that results in a reconfigured antenna capable of radiating with either Right-Hand Circular Polarization (RHCP) or Left-Hand Circular polarization (LHCP). The antenna geometry and parametric configuration are shown in Figure 5.

The work in [17] focuses on the concept of slot antennas, excited by a Co-Planar Waveguide (CPW) line. Figure 6(a) shows the antenna configuration with four switches for operation at the lower frequency, whereas Figure 6(b) shows the antenna

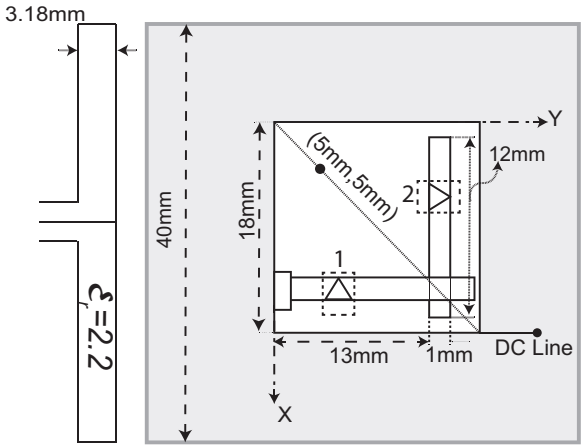

Figure 5. Switchable slot reconfigurable patch antenna dimensions [16].

design in the shortening of other 4 switches out of the total (8) switches. The slot antenna is switched in or out using the PIN diodes for frequency reconfigurability.

The FET switches have also been considered as a strong candidate for achieving the antenna reconfigurability. The first UWB reconfigurable antenna prototype was presented in [18]. Gallium Arsenide (GaAs) FETs were used to connect various types of stubs for feeding structures of a monopole. This connection results in different electrical lengths thus re-routing the current paths in radiating elements and making the antenna reconfigurable on multiple bands. The proposed geometry of the reconfigurable antenna in [18] is shown in Figure 7. The Photo Voltaic (PV)

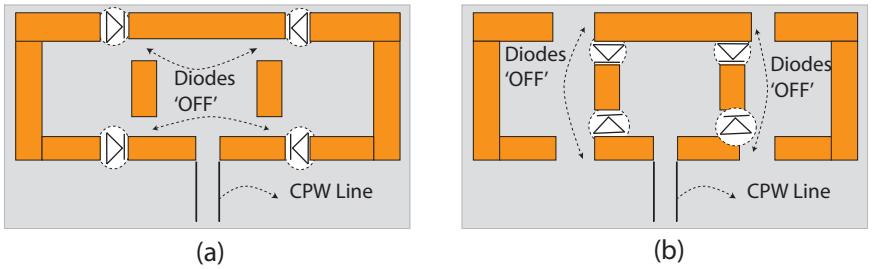

Figure 6. (a) Configuration for a lower frequency and (b) configuration for operation at a higher frequency. [17].

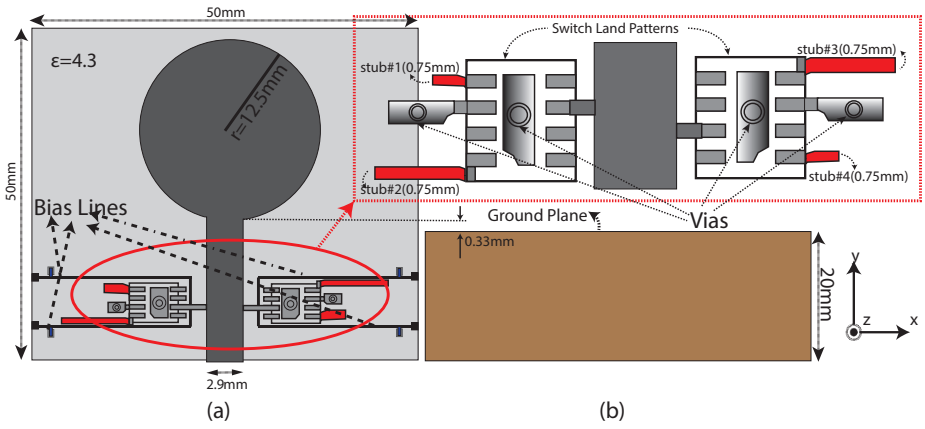

Figure 7. UWB antenna geometry (a) top view and (b) bottom view. [19].

FET characteristics, its operation for RF/μwave switching and intention of the PV FET is also discussed in [19].

1.4. Conducted Research

The re-configurable antennas using existing technologies, such as the RF MEMS, PIN diodes, and the FETs have been explained in the chapter 1. The information presented summarizes the research in the field of reconfigurable antennas, but there are some antennas in literature in which it is difficult to incorporate the biasing network and RF chokes in order to achieve reconfigurability. Therefore, there is a room for significant research to be conducted in the reconfigurable antenna field. The next subsections will explain the research carried out and technical objective of this research.

1.4.1. Properties of Interest and Research Questions

The RF and microwave switches have extensive use in antennas and electromagnetics for switching the frequency, radiation pattern, and the polarization. These switches can be categorized in two main groups; Electromechanical and Solid State

Switches. Moreover, these groups fall into three main forms that are used in RF applications: RF MEMS, PIN diodes, and the FET technology. These existing switches have their own advantages and disadvantages.

The RF MEMS switches have a wide range of applications ranging from cell mode switches in terms of frequency, radiation pattern, and polarization reconfigurability to radar systems. The RF MEMS have low insertion loss and low control power allowing the switch to optimize the power requirements of the system. On the other hand, these switches have high losses at microwave and mm-wave frequencies. These switches may need an inexpensive packaging to protect the moveable MEMS bridges against the environment.

The PIN diodes are also used as an alternative for the applications in antennas to achieve reconfigurability. The PIN diodes have fair microwave performance by providing resistance ranging from a fraction of an ohm when forward biased, to greater than 10 kW [20] when reversed biased. The PIN diodes are suitable for high frequencies but have a limitation when operated down to DC and also require more current to operate [20]. Moreover, FET biased resistance is higher than PIN diodes, this offers high insertion loss [20].

The FET schematic diagram is shown in Figure 8(a). The gate voltage is directly proportional to the conducting channel's size beneath the gate. Thus, by increasing the voltage at the gate increases the conducting channel's size which allows current to flow between the source and drain.

The PIN diodes are heavily doped p-type and n-type regions (used for ohmic contacts), which are doped by a lightly-doped intrinsic region as shown in Figure 8(b). The PIN diodes in forward biasing create a very low resistance at low frequency, while the reverse biasing results in an open circuit. PIN diodes are current controlled, while the FETs require only a voltage signal for switching, instead of a DC current.

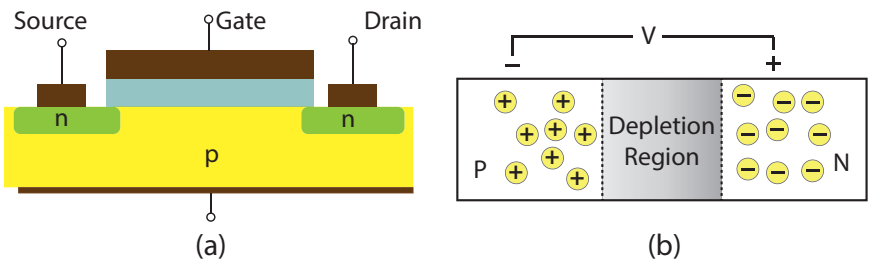

Figure 8. (a) A diagram of a FET (b) A diagram of a PIN diode. [21].

PIN diodes are also capable of controlling large RF signal powers while using much smaller levels of control power. The figure-of- merit of the PIN diodes is higher than the FETs [21].

All of the electrostatic switches discussed earlier have advantages and disadvantages in terms of switching time, drawing current, power loss, and insertion loss. Many reconfigurable antennas have been investigated in literature using these electrostatic components. All of these switches either employ mechanical activation for the movement of radiating elements or radiating elements are kept stationary. The switches are then integrated to alter the electrical length of antenna for re-routing the current path to make it reconfigurable. Antenna reconfigurability using these techniques have been briefly discussed in literature review section of this chapter.

All of the RF switches require a biasing network for their operation and are well characterized in terms of their properties [22]- [23]. In simulations some types of antennas can be made reconfigurable as it may require only a conducting strip for the current continuation path. But when these antennas are manufactured for measurements it is required to activate PIN diodes/FETs/RF MEMS switches by incorporating a biasing network on the antennas substrate. All of these RF switches that are used for antenna reconfigurability require a DC power for their operation and

this addition of DC power may add some bulkiness and cause degradation in antenna performance.

Thus the proposed research will be focusing on the following two points.

- If a switch is designed such that it can be activated using magnetostatic fields, then what will be its impact on the RF power and how will this magnetic switch will be characterized in terms of its S-parameters (insertion loss and isolation in the 'OFF' state)?

- How will these proposed magnetic switches be used in achieving reconfigurability and will they be a good alternative for the antennas that are difficult to reconfigure using conventional MEMS/PIN diodes/FETs?

1.4.2. Technical Objectives

1. Model and test the idea of MEMS based RF magnetic switches in 3-D Electromagnetic simulator High Frequency Selection Simulator (HFSS) [24]. Manufacture micro level magnetic switches and investigate the characteristics of the magnetic switch, such as S-parameters and insertion loss, on a known microstrip transmission line.

2. Investigate the simulation model of the proposed magnetic switch and simulation of different types of reconfigurable antennas using magnetic switch in 3-D Electromagnetic simulator High Frequency Selection Simulator (HFSS) [24], and Advanced Design Software (ADS) [25].

3. Verify the results of the simulated reconfigurable antennas with the measurement results by incorporating the manufactured magnetic switch prototypes. Especially in the antenna where polarity issues arise and become difficult to use a diode for achieving switchable multi-band operation.

1.5. Previous Work on Magnetic Switch Development and Feasibility Study

1.5.1. Introduction

An initial investigation and feasibility study of the magnetic switch development will be discussed in this subsection. The portion of this chapter will focus on the manual manufacturing of magnetic switches (1st Generation (Gen.) switches). The 1st Gen. switches behavior in the Radio Frequency (RF) field will be further explored along with effect of magnetic field strength analysis on the proposed switch. The RF response of the initial magnetic switch prototypes will also be presented.

1.5.2. Feasibility Study of the Magnetic Switch

An initial investigation was conducted by the preliminary experimentation to verify the idea of the magnetic switch. The switch consists of two parallel plates with a dielectric layer between them. Figure 9 shows the schematic of the proposed switch. The top electrode is a soft Copper (Cu) sheet, whereas the bottom electrode is a standard Cu-clad FR4 board. The dielectric is a 125.0 micron thick kapton. The cavity in the kapton is made using the standard office punch and has a diameter of 7.0 mm. Ni-coated particles [26] (Figure 10) having an average size of 40.0 microns, are filled in the cavity of dielectric portion as shown in Figure 9. Dimensions of the

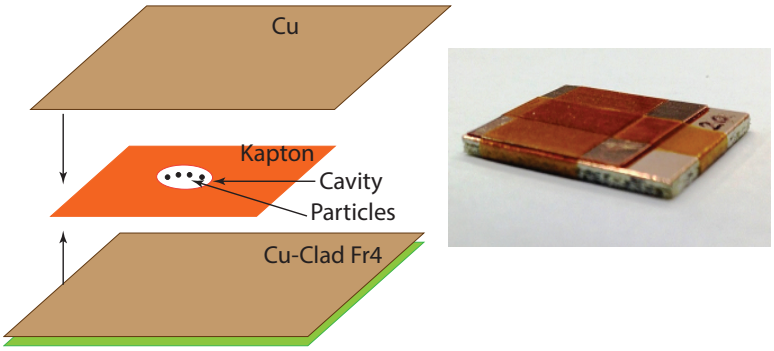

Figure 9. Magnetic switch first prototype, switch parts schematic (*left*) and assembled switch (*right*).

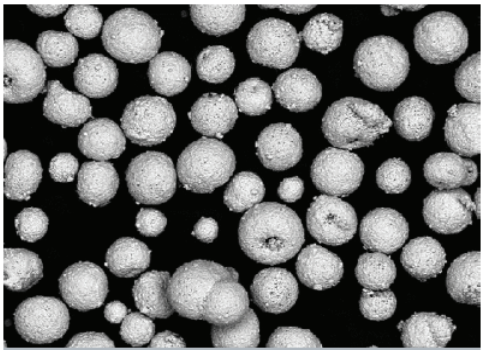

Figure 10. Silver coated magnetic additive, CONDUCT-O-FIL SM40P 20.

first prototype are shown in Figure 11. When this proposed structure is brought in between the two static magnets (6.0 mm apart from proposed switch structure) the resistance is 50 Ω. The switch behaves as a 'short' (low resistive path) by aligning the magnetic particles whereas in the absence of magnetic field, the switch acts as 'open'.

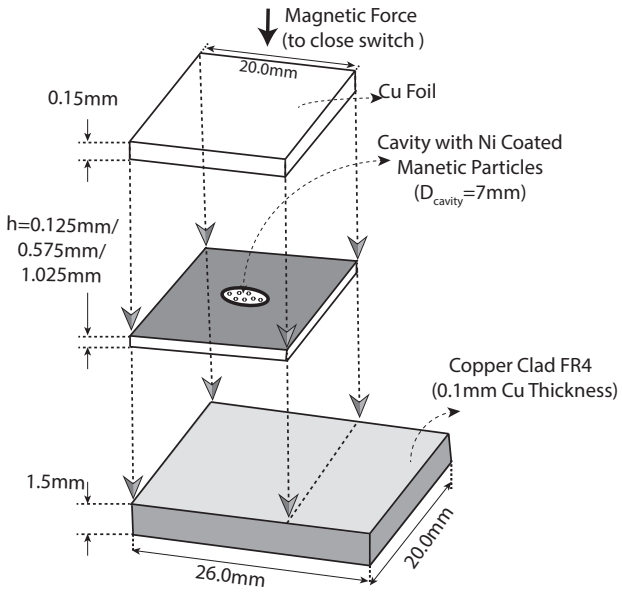

Figure 11. Dimensions and structure of first prototype switch.

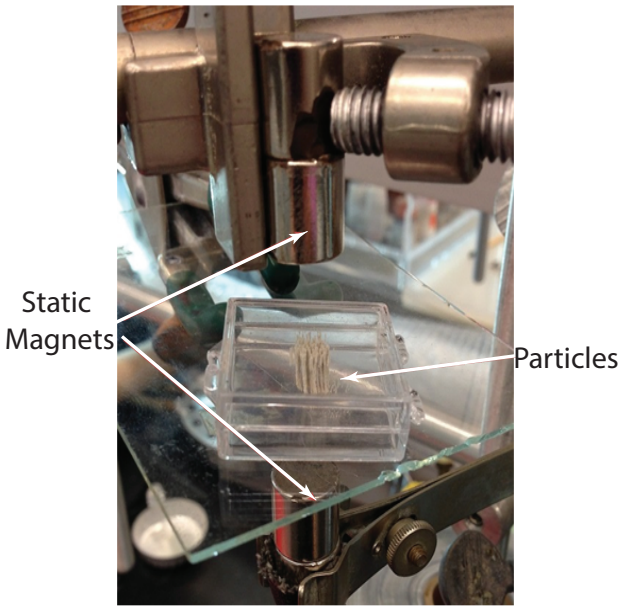

Figure 12. Magnetic particles in a transparent box placed between two magnets.

In a separate observation experiment, a small amount of magnetic particles are placed in a 7.0 mm thick plastic box and the magnetic field is applied to witness the particles behavior. As the magnets are aligned together, the particles start to concentrate and build a column in the center of the box, as shown in Figure 12. The distance between the magnets is 36.0 mm, corresponding to the magnetic field strength of 500 Gauss. This experimental verification shows that the MEMS based magnetic switches can be a possible replacement for other DC biased RF switches and do not require a direct connection. In the next step [29] additional structures with more controlled amounts of particles were built and tested to observe their behavior (resistance) with a constant magnetic field initially.

1.5.3. Magnetic Field Strength Analysis

The magnetic field strength was varied by changing the distance between the two static magnets. The strength of the field was measured at the mid-point between the two magnets using a gauss meter. The strength of the magnetic field with respect

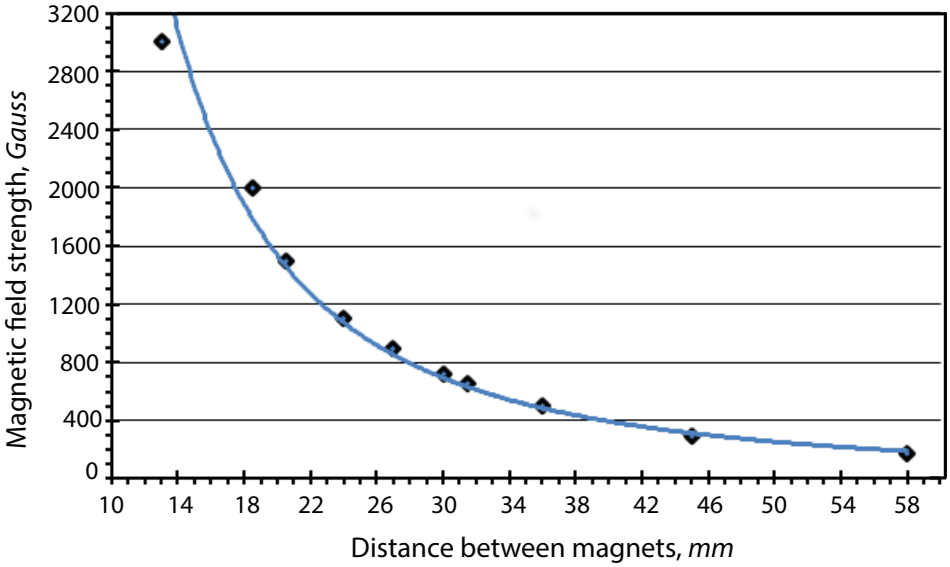

Figure 13. Magnetic field strength vs distance between the magnets [29].

to the distance between the two magnets is shown in Figure 13; black diamonds are measured values, whereas black line is a curved fit [29].

1.5.4. Quantification of Particles

In order to quantify the amount of particles in each individual switch, a value R was introduced [29]. The R-value is equal to the ratio of the volume of the cavity to the volume of the particles in the cavity. This R value is used to ensure that the cavities with different depths (hence different volume) each receive the right amount of particles, i.e. a cavity with a smaller depth (volume) will be filled with smaller amount of particles than a cavity with a larger depth, but both will have the same R value. The R-values that were used were 20.2, 28.9, 40.4, 50.5, 67.3, and 101. So, for example, a switch with an R = 20.2 has a cavity volume 20.2 times larger than the volume of the particles in it, and a switch with R value of 101 has less particles than the switch with R = 20.2. The behavior of these switches was studied in a magnetic field that varied from 300 to 3000 Gauss and the objective was to

observe how fast the resistance dropped as the magnetic field strength increased and at what point did the overall resistance of the switch (measured between the top and bottom electrode) fell in the low Ohm range, i.e. less than 10 Ω. It was observed that as the amount of particles in the cavity is increased, the switch resistances in magnetic field approaches the lower values faster; this makes sense, as more particles are available to form columns. The resistance behavior as the R-value decreases is also discussed and observed that the amount of particles increases, for different magnetic field strength [29].

The behavior of the resistance of these switches in the presence of magnetic field is reported in [29]. It is reported that the switches with a higher volume, hence higher height (diameter was fixed), approached the low resistance values faster and showed more stable behavior than switches with lower volume/height with the same R-value. Upon closer inspection of particle behavior, it was seen that as the magnets are brought together, the particles first redistribute to cover the whole area of the magnetic field, and as the field is increased they start to 'climb' on each other to form columns. That means, although a switch with fewer particles may have the same

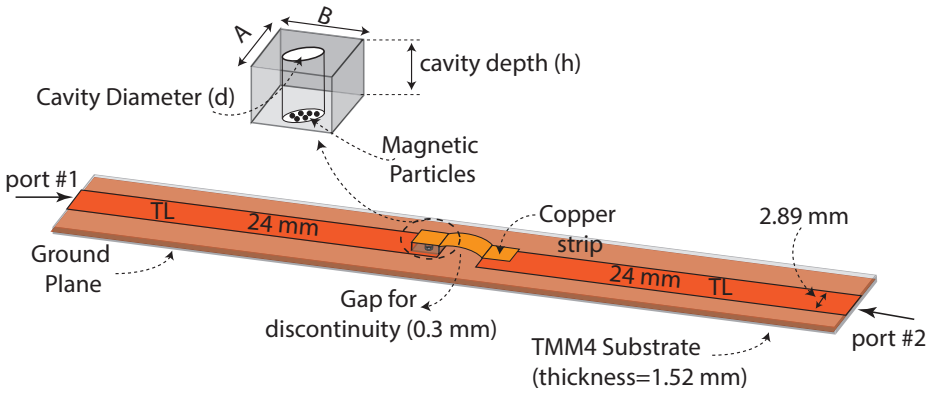

Figure 14. Dimensions (all in mm) magnetic switch build on a 50-Ω transmission line. For first prototype A = 20, B = 20, h = 0.125, and d = 7. For smaller switches A = 1.5, B = 1.5, h = 0.508/1.52/3.08, and d = 1.5.

R-value than a switch with more particles, the first will have fewer particles to start forming columns in the same cavity diameter. Therefore, to reduce the field needed to close the switch, it is necessary to decrease the area of the magnetic field (make it more concentrated), or to reduce the area of the switch cavity.

1.5.5. 1st Gen. Magnetic Switch Behavior in the RF field

To study the behavior of a magnetic switch in an RF field, magnetic switch prototypes were attached to a 50-Ω microstrip transmission line for the preliminary evaluation. A detailed illustrative drawing of the magnetic switch with the dimensions of the cavities and overall switch size with the interconnecting 50-Ω microstrip TL is shown in Figure 14. Initially, a bigger prototype with a 7.0 mm cavity diameter was tested (Figure 16 (b)) and the RF field response measurements using a network analyzer is shown in Figure 15.

The RF field response measurement of the magnetic switch is shown in the Figure 15. It was shown that the results are promising due to the fact that the switch is changing between two states when the magnetic field is applied. The larger

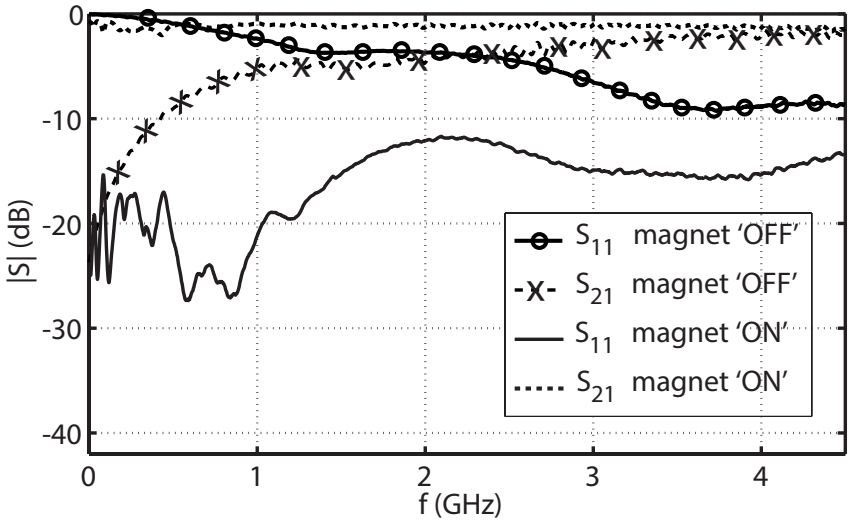

Figure 15. RF field response measurement (S-parameters) of initial prototype on a 50-Ω TL.

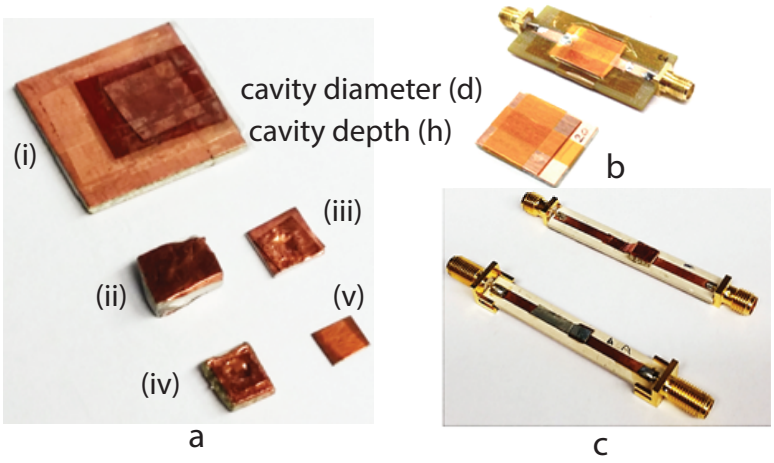

Figure 16. (a) Magnetic switch prototype (bottom) and big switch prototype (top) on a 50-Ω TL, (b) magnetic switch prototypes (i) h = 0.125 mm, d = 7 mm, (ii). h = 3.05 mm, d = 1.5 mm, (iii) h = 0.508 mm, d = 1.5 mm, (iv) h = 1.52 mm, d = 1.5 mm, and (v) h = 0.125 mm, d = 1.5 mm, and (c) smaller magnetic switch prototypes on a 50-Ω TL with d = 1.5 mm, h = 0.125 mm (top) and d = 1.5 mm, h = 1.52 mm.

manufactured magnetic switch was able to switch the transmission on a TL up to 500 MHz (isolation of less than −10dB) while maintaining a good impedance match in the 'ON' state (i.e. in the presence of magnetic field). It was observed that there is capacitive effect due to the larger cavity diameter (h) and larger area of the magnetic switch. Minimizing the capacitive effect can increase the isolation cut-off frequency of the magnetic switch. The capacitive effect can be minimized by decreasing the area of the switch, using low epsilon substrate, or by decreasing the cavity depth (h) of the switch. In order to observe this change, smaller magnetic switches were manufactured.

Figure 16 (a) shows the smaller magnetic switches whereas, switches on a 50-Ω TL are shown in Figure 16 (c). Figure 16 shows the 1st Gen. larger and smaller manufactured magnetic switches on a 50-Ω TL. The $|S_{21}|$ of these smaller prototypes

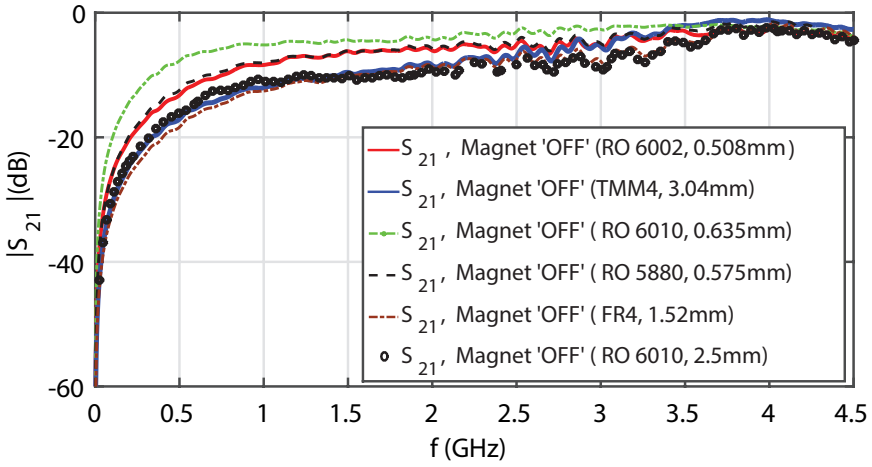

Figure 17. RF field response measurement ($|S_{21}|$) of switches having different cavity depths (h) and substrates on a 50-Ω transmission line.

with different cavity depths (h), and different substrates in the 'OFF' state are shown in Figure 17. Only 'OFF' state $|S_{21}|$ are shown, as the capacitive coupling was present only in 'OFF' state. In the 'ON' state the RF behavior of these switches were same as shown in the Figure 15. It can be observed that there is switching capability increase up to 1.5 GHz (isolation less than −10 dB) for smaller switches with different cavity depths and substrates.

1.6. Conclusions

In this chapter a literature review on the reconfigurable antennas was presented. A descriptive overview on the working principles of the FETs and PIN diodes was also explored. It is concluded that PIN diodes, RF MEMS, and FETs require a DC biasing circuitry for their operation on a RF platform. Based on the limitations of these RF switches for achieving reconfigurability in some antennas, research questions and technical objectives of this research work were proposed. Moreover, an initial prototyping of the magnetic switch with a larger cavity, its RF response on a 50-Ω TL and magnetic strength analysis was discussed in this chapter. Based on the results,

switches with smaller diameter were built and their behavior was studied. Their behavior in RF field showed that smaller switches have better switching capabilities and weaker magnetic field is need to close the switches. If that trend extends to the micron sized switches, switching capabilities can be increased above 1.5 GHz and even less amperage will be needed in biasing the magnetic switch. It is concluded that magnetic switch can be used as RF switching and there is a need of proposing a refined quantification method of magnetic particles for micro level switches.

CHAPTER 2. DEVELOPMENT AND CHARACTERIZATION OF MICRO SIZED MAGNETIC SWITCHES

2.1. Introduction

An accurate manufacturing of the micro switches and cavities in which particles will be placed is presented in this chapter along with the modeling of the switch geometry in HFSS v. 15.0 [24]. Moreover, a more accurate way of quantifying magnetic particles will be described followed by the RF field behavior and characterization of the micro level magnetic switches (2nd Generation (Gen.)).

2.2. Fabrication and Manufacturing of The 2nd Gen. Magnetic Switches

A ProtoMat S63 masters 2.5-dimensional [30] PCB milling machine was used to manufacture the micro level switches and accurate manufacturing of the cavities. In particular, the milling practices were used to make cavities in a substrate and for the accurate cutting of 2nd Gen. switches. Initially, a 0.9 mm cavity diameter (d) switches having an overall size of 3.0 mm $\times$ 3.0 mm $\times$ 0.508 mm (i.e. a 3.0 $\times$ 3.0 mm^2 on a 20 mil or 0.508 mm (h) substrate) were accurately manufactured. The substrate material used was TMM4 and had 1 oz copper on both the top and bottom layer. These switches are shown in the Figure 18 (a).

A photograph of manufactured switches in Figure 18 (a) shows that milling practice for switch fabrication is feasible and even smaller switches can be manufactured. Figure 18 (b) shows the manufactured prototype cavities with a diameter of 0.4 mm, thickness of 20 mils, and a square copper (1 oz) and substrate size of 1.0 mm $\times$ 1.0 mm whereas cavities having a diameter of 0.9 mm and area of 1.5 mm $\times$ 1.5 mm are shown in the Figure 18 (c). Switch A in the thesis will refer to the magnetic switch dimensions shown the Fig. 18 (a), whereas Switch B will refer to the magnetic switch shown the Fig. 18 (c).

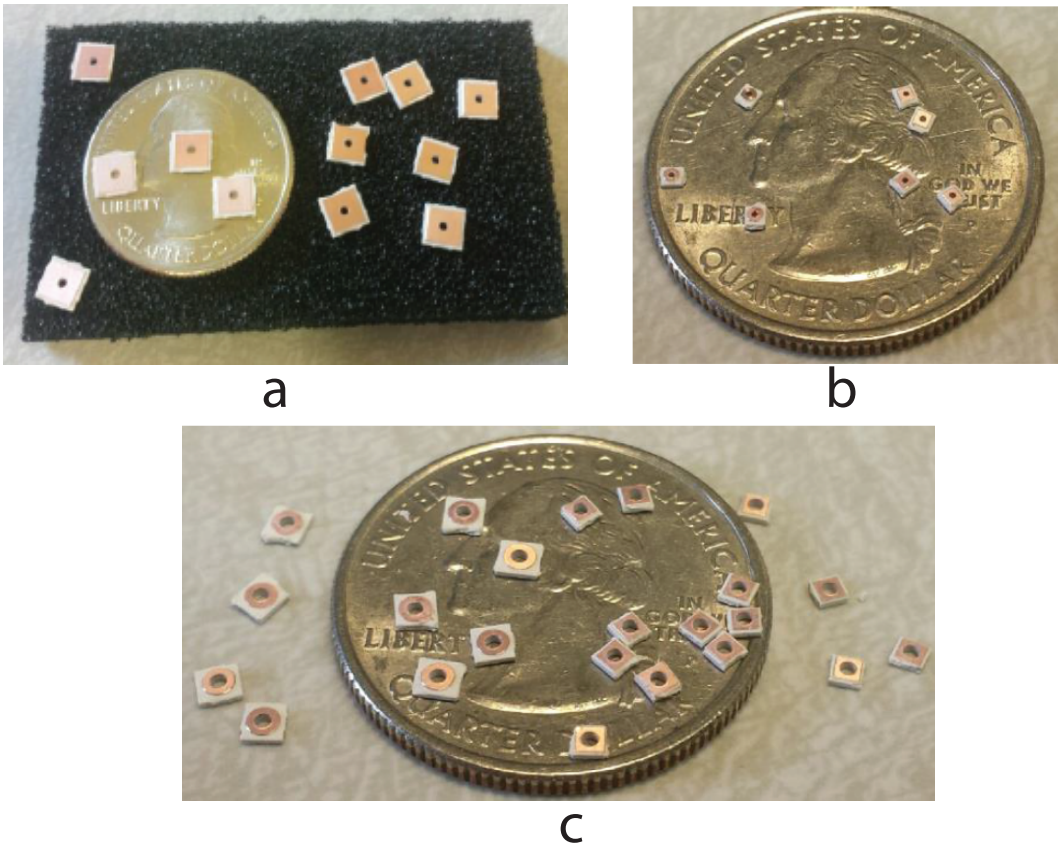

Figure 18. Manufactured magnetic switch cavities using milling machine, (a) d = 0.9 mm, h = 0.508 mm, and area = 3.0 × 3.0 mm^2, (b) d = 0.4 mm, h = 0.508 mm, and area = 1.0 × 1.0 mm^2, and (c) d = 0.9 mm, h = 0.508 mm, and area = 1.5 × 1.5 mm^2.

2.3. Quantification of Silver Coated Particles

After the manufacturing of the cavities for the silver coated particles (microscopic image is shown in Figure 19), the cavity shown in Figure 18 (a) was filled with calculated amount of particles. The number of individual particles placed in the cavity were counted with a microscope. The cavity filling results for 11 and 43 particles are shown in Figure 20 (a) and (b), respectively. However, when the switch was placed between the permanent magnets the magnetic particles were not able connect the bottom copper with the top copper tape.

Figure 19. Microscopic view of the particles.

Then the cavity was filled with even more particles for the purpose of checking of the test set-up. Figure 20 (c) shows the microscopic view of amount of particles, and it can be seen that it is becoming hard to count the exact number of particles. With this amount of particles in the switch, the switch was not able to provide a connection in the presence of a static magnetic field. Additional particles (Figure 20

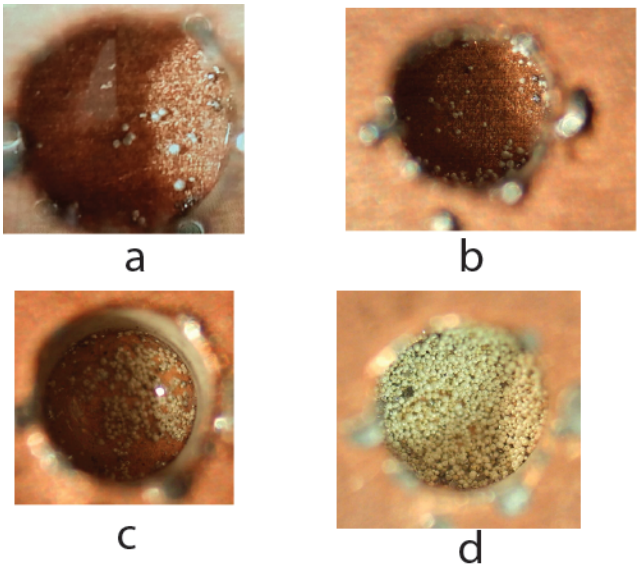

Figure 20. (a). Cavity with 11 particles, (b) cavity with 43 particles, (c) magnetic switch with more then 43 particles- 1^{st} iteration, and (d) magnetic switch with more then 43 particles- 2^{nd} iteration.

(d)) were then added to the cavity with the pipette. At this point, there were enough particles in the cavity to connect the two conducting planes.

The above experimentation of counting the magnetic particles in the cavity showed that the particles were closely packed in the cavity, and it became harder to estimate the exact amount of particles. However, the particles when they are not closely packed can be counted in a cavity or on a plane sheet. So, particles counting is possible, if the surface is large so that particles can spread out on that surface for counting.

2.3.1. Counting of Silver-coated Particles

A measuring cup having a cavity diameter of 0.4 mm and thickness of 0.015 inches (0.254 mm or 15.0 mils)is manufactured (as shown in Fig. 21). The amount of particles than can fill the manufactured cylindrical cavity was first estimated mathematically, as

$$V = \pi r^2 h. \tag{2.1}$$

Here, V is the volume, r is the radius, and h is the height of the cylindrical cavity. For the measuring cup the volume V of the cavity was 2.92×10^{-6} inches^3. Similarly, the volume K of the a spherical magnetic particle having an average radius of 7.87×10^{-4} inches (20.0 micron) was calculated using,

$$K = \frac{4}{3}\pi R^3, \tag{2.2}$$

where R is the radius of the magnetic particle. The calculated volume of a magnetic particle was 2.0449×10^{-9} inches^3. In spherical packing, the densest possible arrangement of spherical particles in a three-dimensional cylindrical enclosure has been well addressed by Kepler and is commonly known as Kepler's problem [27]. So

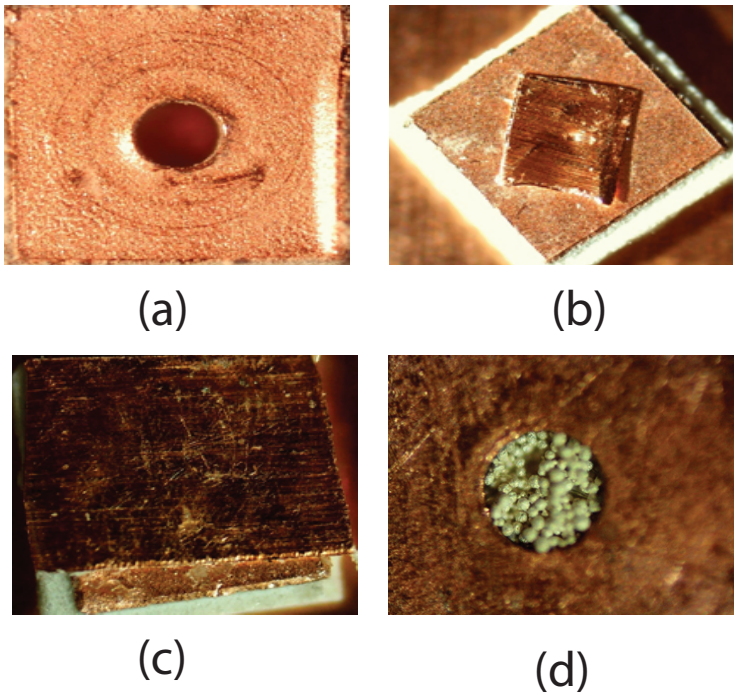

Figure 21. (a). Measuring cup, (b) copper sheet on bottom side, (c) copper tape on bottom side , and (d) measuring cup filled with magnetic particles.

the density of spherical particles having a volume K in volume V was calculated by using Kepler's formula [27], i.e.:

$$\eta = \frac{\pi}{3\sqrt{2}} = 0.74048. \tag{2.3}$$

This implies that 74 % of available space will be occupied by the spherical particles and 26 % by the air in the measuring cup. Then the total number of particles in the cavity was estimated using

$$N = 0.74\frac{V}{K} \cong 1056. \tag{2.4}$$

So, a measuring cup having a diameter of 0.45 mm and a cavity height or thickness of 0.254 mm (15.0 mil) can hold 1056 particles.

The estimated number of particles calculated analytically was then verified by filling a measuring cup with the magnetic particles and then experimentally counting the magnetic particles. In order to count the magnetic particles, the measuring cup was filled with the magnetic particles. A microscopic view of the measuring cup is shown in the Figure 21 (a). A small piece of copper sheet was placed on the bottom side of the cup as shown in Figure 21 (b), and a copper tape having same size of the measuring cup was used on the top of copper sheet to hold the particles (Figure 21 (c). The purpose of the small copper sheet was to avoid the sticking of particles to the copper tape and minimize the counting error. These filled magnetic particles are then transferred from this cavity on a flat piece of sheet by pacing a small magnets under the flat piece of sheet. The flat sheet was placed under a microscope and magnetic particles were counted. This procedure was performed five times and number of particles were counted for each experiment. The counted particles were found to be approximately 1010, 950, 1080, 1125, and 1050 for five experiments, respectively. So, a measuring cup (shown in Figure 21 (a)) can hold up to 1050 particles having an error of ± 50.

Once the counting of particles using the measuring cup was done, then these particles are migrated onto a manufactured magnetic switch by drilling a small hole on the flat sheet containing the calculate and counted of particles. An illustrative drawing of showing particle migration to the cavity is shown in Figure 22. The hole of the sheet was placed on the top of magnetic switch cavity and a small permanent magnet was used to move the particles and place them in the magnetic switch. It can argued that a magnetic switch will have approximately 1050 number of magnetic particles if one scoop of the measuring cup was used to fill the magnetic switch.

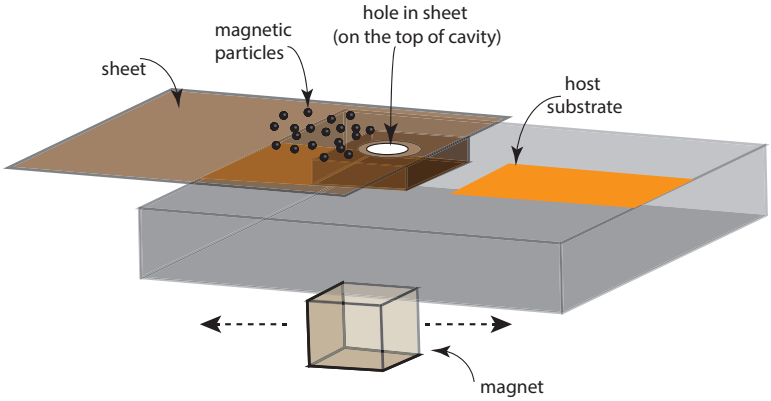

Figure 22. Method used to migrate the magnetic particles in the cavity.

2.4. Characterization of the Magnetic Switch

After the quantification of magnetic particles in a magnetic switch, the S-parameters of the magnetic switch were extracted to identify the operational and frequency characteristics of the micro level magnetic switches in the RF applications.

2.4.1. Procedure for Extracting S-parameters

In order to extract the insertion loss (S_{21}) of the magnetic switch in the 'ON' state and isolation (S_{21}) in the 'OFF' state, a discontinuous 50-Ω TL with a gap of 0.3 mm, having a dimension of 5 $mm \times 5$ mm on a TMM4 substrate (1.52 mm) was manufactured, and the magnetic switch was placed in the gap. A prototype of the TL with the magnetic switches having approximately 1050 magnetic particles in the cavity is shown in the Figure 24. Detailed dimensions of the prototypes used for the S-parameters extractions is shown in Figure 23.

The S-parameters, $S_{Overall}$ (magnitude and phase), of the prototypes shown in Figure 24 were measured using a calibrated network analyzer E5071C (100 KHz-4.5 GHz) in the switch 'ON' and 'OFF' states. These measured S-parameters were then converted in to ABCD parameters using standard conversion formulas [28]. Mathematically,

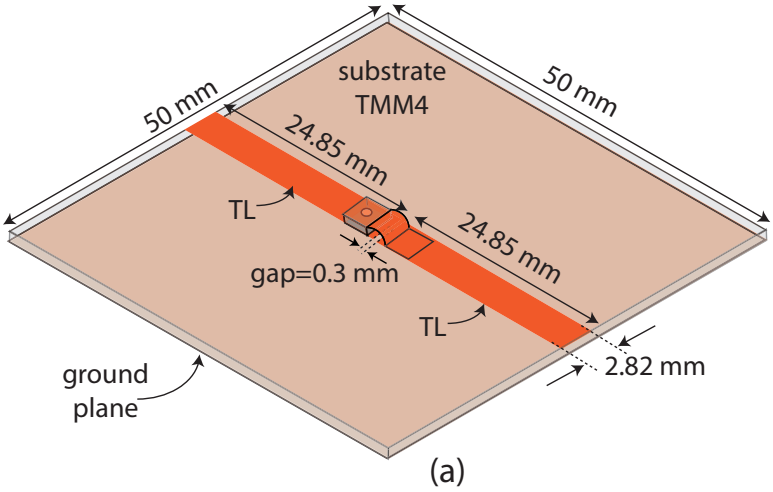

Figure 23. Dimensions of a 50-Ω TL with magnetic switch prototype used for the S-parameters extraction.

$$S_{Overall} = \begin{pmatrix} S_{11_{overall}} & S_{12_{overall}} \\ S_{21_{overall}} & S_{22_{overall}} \end{pmatrix} \tag{2.5}$$

and

$$ABCD_{Overall} = \begin{pmatrix} A_{overall} & B_{overall} \\ C_{overall} & D_{overall} \end{pmatrix}. \tag{2.6}$$

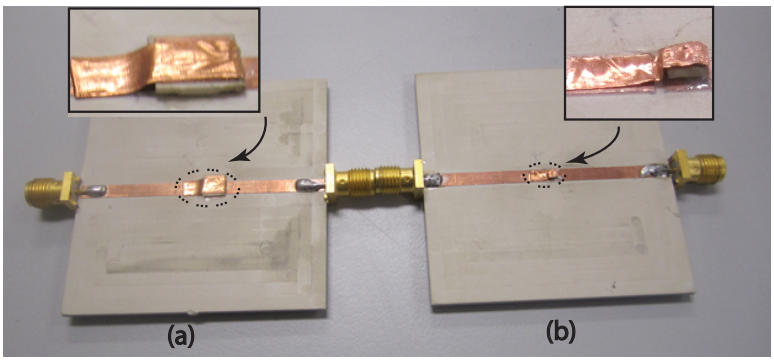

Figure 24. (a) Switch A on a 50 Ω discontinuous TL, (b) switch B on a 50 Ω discontinuous TL.

The S-parameters, $S_{Left\ half}$ and $S_{Right\ half}$ of the half TLs were then measured and converted in to $ABCD_{Left\ half}$ and $ABCD_{Right\ half}$, respectively. After the ABCD conversion and using the ABCD property that ABCD parameters of the systems multiply in the cascaded systems, the ABCD parameters of the switch were extracted in the switch 'ON' and 'OFF' state. Mathematically,

$$ABCD_{Overall} = ABCD_{Lefthalf} \times ABCD_{Switch} \times ABCD_{Righthalf} \tag{2.7}$$

and

$$ABCD^{-1}_{Lefthalf} \times ABCD_{Overall} \times ABCD^{-1}_{Righthalf} = ABCD_{Switch}. \tag{2.8}$$

After the computation of $ABCD_{Switch}$, the insertion loss of the magnetic switch in the 'ON' state and isolation of the magnetic switch in the 'OFF' state were computed.

2.4.2. Results and Discussion

The insertion loss of the magnetic switches (Switch A and Switch B) in the 'ON' state is shown in Figure 25. It can be seen from the Figure 25 that in the 'ON' state

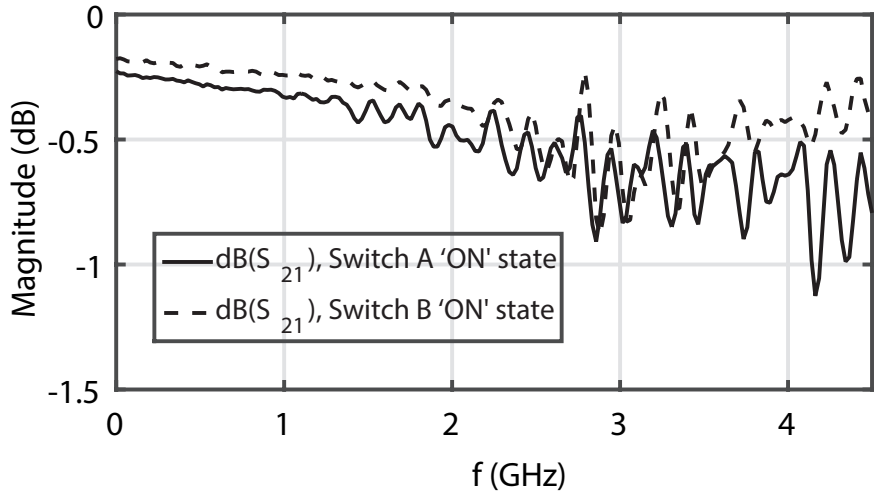

Figure 25. Insertion loss magnetic switches (Switch A and Switch B in the 'ON' state.

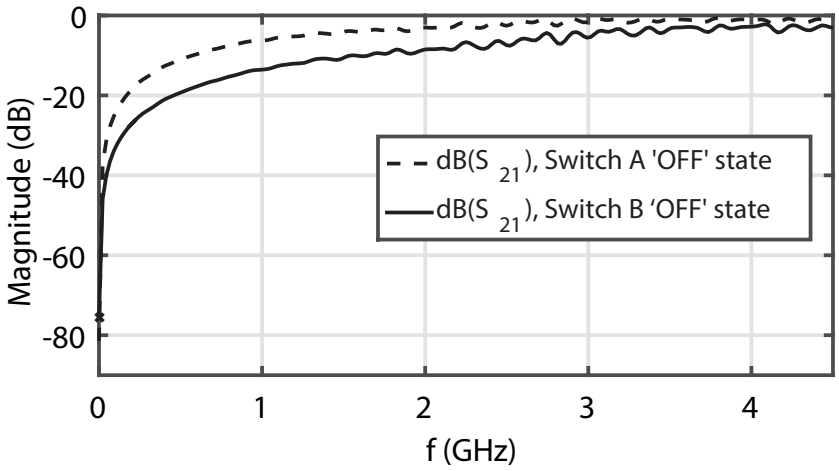

Figure 26. Isolation of the magnetic switches (Switch A and Switch B in the 'OFF' state.

both switches have an insertion loss less then 1.5 dB. However, Switch B has lower insertion loss, but the general behavior of the insertion loss is the same for both the switches. At lower frequencies, the insertion loss is less then 0.5 dB, and, then, at higher frequencies, there is an increase in the loss up to 1.5 dB. Overall, both the switches have good insertion loss and the switches are capable of propagating EM waves over the range of frequencies from 100 KHz - 4.5 GHz.

Figure 26 shows the isolation of the magnetic switches in the 'OFF' state. It is shown in Figure 26 that Switch A is capable of providing an isolation of 10 dB up to several 100 MHz, whereas isolation performance of the Switch B is better as compared to the Switch A. Switch B has 10 dB isolation up to 2.6 GHz.

The S-parameter results of the micro level magnetic switches showed that the switches have better operation and frequency characteristics, thus these micro-level switches can be used in the RF switching.

2.5. Magnetic Switch Simulation Model and Behavior in the RF Field

A simulation model of the magnetic switch (Switch A) with a 50-Ω TL was then modeled in HFSS v.15.0 [24]. Figure 27 shows the geometry of the magnetic

switch and TL modeled in the simulation software. In simulation, the magnetic switch 'OFF' state was modeled by placing the spheres on the bottom of the switch cavity. The 'ON' state of the switch was modeled by modeling columns of magnetic particles having an average diameter of 40.0 micron to provide a connection between the bottom and top copper tape of the switch.

In order to analyze the S-parameters variation of the magnetic switch 'ON' state a simulation on numbers of columns of the magnetic particles was done. S_{11} results for the 1, 2, 4 and 25 number of columns are shown in the Figure 28. It can be observed that as the number of columns are increased, the S_{11} values are less then -10 dB (the same S_{22} values were obtained). These number of columns do not effect the S_{11} and S_{22} (dB) values over the range of frequencies from 100 KHz to 4.5 GHz. These results showed that in simulation model, one number of column can be used to simulate the magnetic switch 'ON' state.

In order to check the validation of the modeled TL with the magnetic switch, TLs having the same dimensions as given in Figure 27 were fabricated, and manufactured magnetic switches were then attached to the prototypes, as shown in Figure 29.

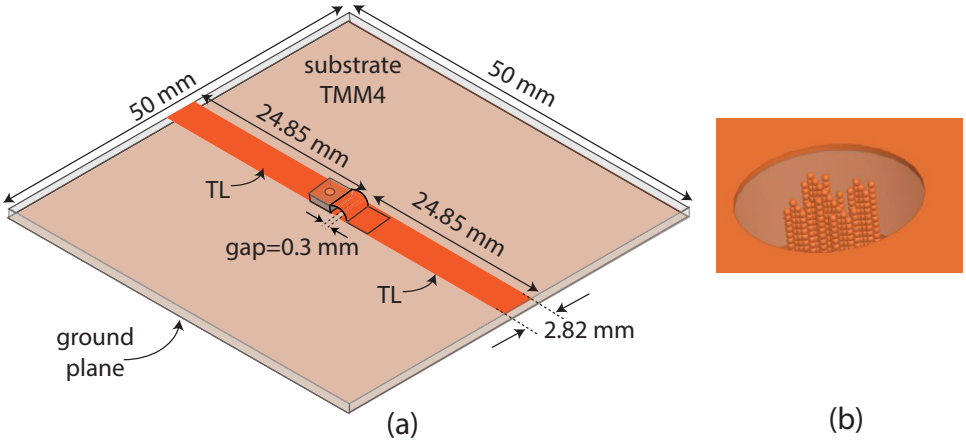

Figure 27. (a) Dimension of a 50-Ω TL with magnetic switch modeled in HFSS v. 15.0 and (b) Magnetic particles model in HFSS.

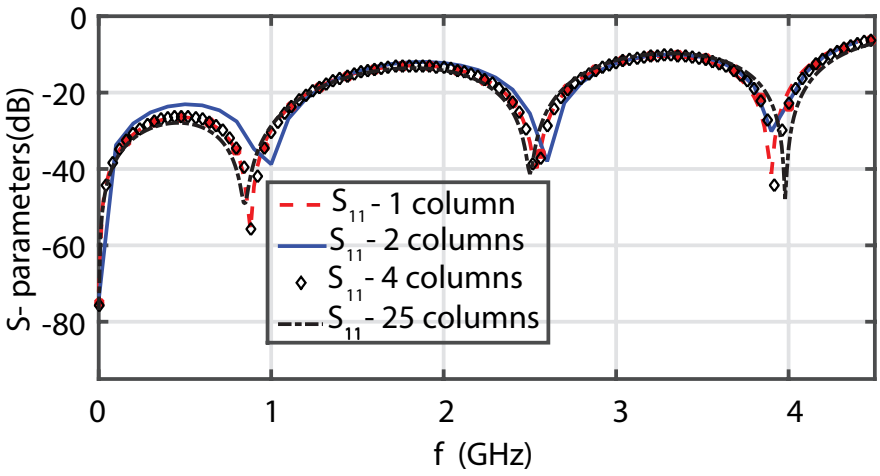

Figure 28. Simulated S_{11} values of magnetic switch for various columns of particles.

These magnetic switches were filled with the magnetic particles using the measuring cup (1050 particles), following the procedure explained earlier. Figure 30 and Figure 31 show the comparison of S-parameters of the manufactured magnetic switch A on a 50-Ω TL with the simulation model. As S-parameters of the simulation model were independent to the various columns of particles in the 'ON' state of the switch, so

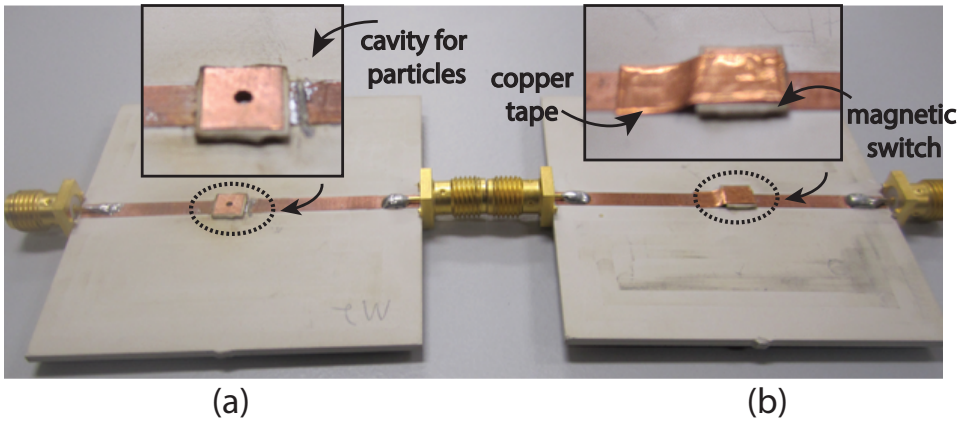

Figure 29. (a). Photograph of the cavity attached to the 50-Ω TL (b). Photograph of the cavity on the host TL with magnetic particles and connected with copper tape.

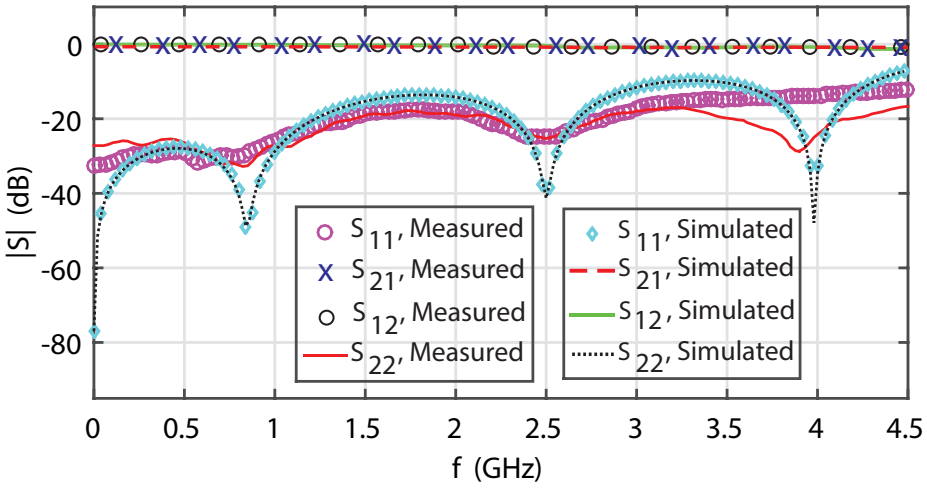

Figure 30. S-parameters comparison of measurements and simulation model ('ON' State).

for simplicity one column of particles was used to compute the results in the switch 'ON' state, whereas in the 'OFF' state only the magnetic cavity (no particles) was modeled in the simulations.

It can be observed from the Figure 30 that in the presence of the magnetic field and a 'ON' (activated) switch, the EM wave is propagating on the TL and S_{11}/S_{22} (dB) values on the ports of TL are less then -10 dB. Overall, simulation and measurement results showed good agreement.

Figure 31 shows a comparison of the simulations and measurements of the switch in the 'OFF' state. It was shown that for both the simulations and measurements Switch A has switching capabilities up to 500 MHz on a 50-Ω TL. There is transmission above 500 MHz through the switch in the 'OFF' state because of the capacitive coupling at higher frequencies.The results showed that the capacitive effect in the presence of magnetic particles (manufactured) was similar to that of absence of particles in simulations. The capacitive coupling effect on the measured results of the magnetic switch in the 'OFF' state is in good agreement with the simulation results of magnetic switch cavity (no particles).

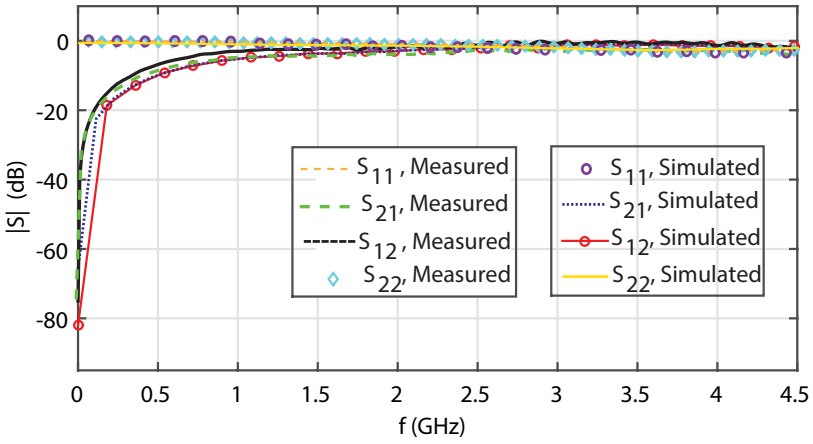

Figure 31. S-parameters comparison of measurements and simulation model ('OFF' State).

Next, smaller switch prototypes having a cavity diameter of 0.9 mm with a square copper size of 1.5 mm x 1.5 mm on a 0.508 mm (20 mil) TMM4 substrate were manufactured. Figure 32 (a) shows the photograph of the smaller cavity (Switch B) attached on a 50-Ω TL, whereas Switch B with magnetic particles attached on a host 50-Ω TL is shown in the Figure 32 (b).

Figure 33 shows the S-parameters of the magnetic switch B on a TL in the magnetically 'biased' and 'unbiased' state of the magnetic switch. It can be observed

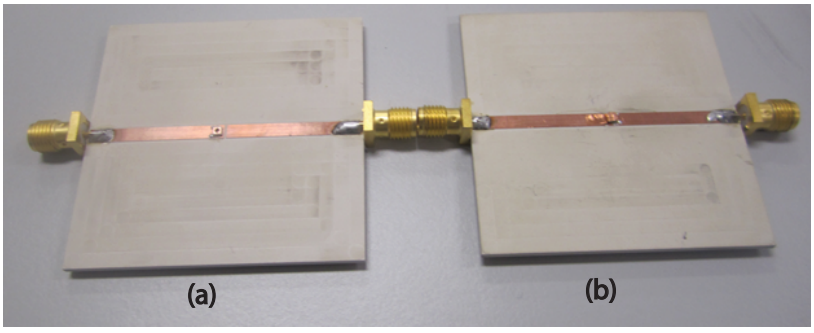

Figure 32. (a). Photograph of the switch B cavity attached to the 50 Ω TL, (b). Switch B with particles on a 50 Ω TL attached connected with copper tape.

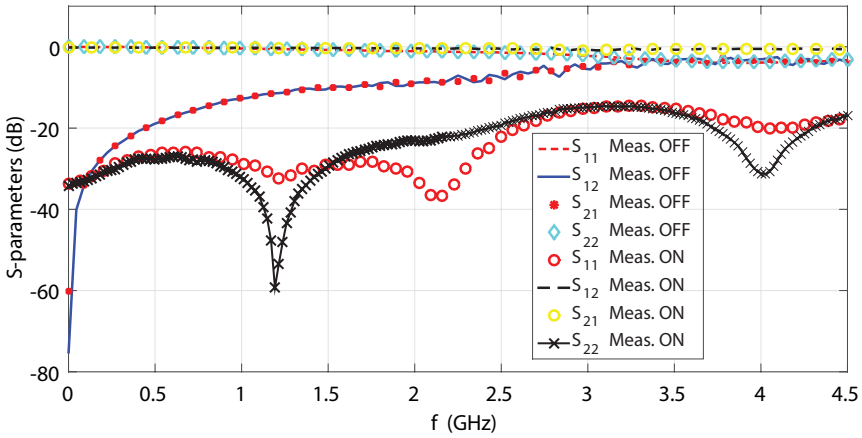

Figure 33. Measured RF response of Switch B on a 50 Ω TL.

from Figure 33 that when the switch is activated (presence of the magnetic field), the EM wave is propagating on the TL and return loss is less then -10 dB. In the 'OFF' state, there is mismatch on the ports of the TL and the -10 dB isolation is up to 1.6 GHz. This shows that the switch is capable of switching for up to 1.6 GHz on a 50-Ω transmission line.

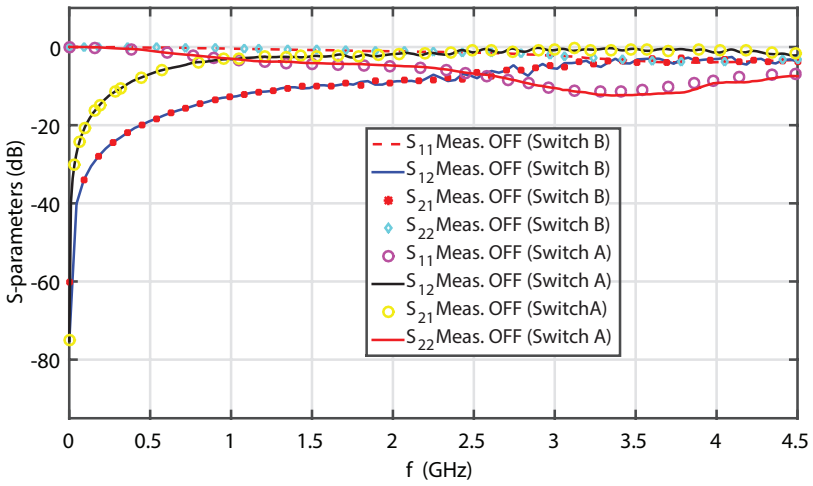

Figure 34. RF field response comparison of Switch A and Switch B on a TL line ('OFF' State).

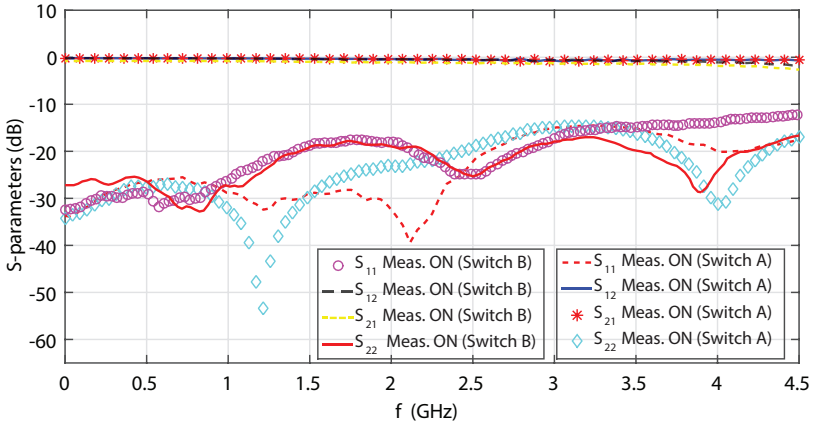

Figure 35. RF field response comparison of Switch A and Switch B on a TL line ('ON' State).

The comparison of the measured RF behavior of Switch A and Switch B in the 'ON' and 'OFF' states on a 50-Ω TL is shown in Figures 34 and Figure 35. It can be observed from Figure 34 that in the 'OFF' state, the return loss is at 0 dB, whereas for the transmission, switch A is capable of isolating up to 500 MHz and switch B is capable of providing isolation up to 1.6 GHz on a 50-Ω transmission line. Thus switching capabilities are increased as compared to switch A on a 50-Ω TL.

The measured RF field response of switch A and switch B in 'ON' state on a TL was also compared and is shown in Figure 35. It was shown that in the 'ON' state, the EM wave is propagating on a TL over a range of frequencies from 100 KHz to 4.5 GHz and the return loss is less than -10 dB.

2.6. Equivalent Circuit Model of the Magnetic Switch

An equivalent circuit of the magnetic switch was extracted using transmission line theory and microstrip discontinuities theory for the better understanding of the RF switching mechanism of the proposed magnetic switch. The bottom of the magnetic switch was connected to the one end of the discontinuous TL, whereas the top surface of the magnetic switch was connected using a copper tape to the

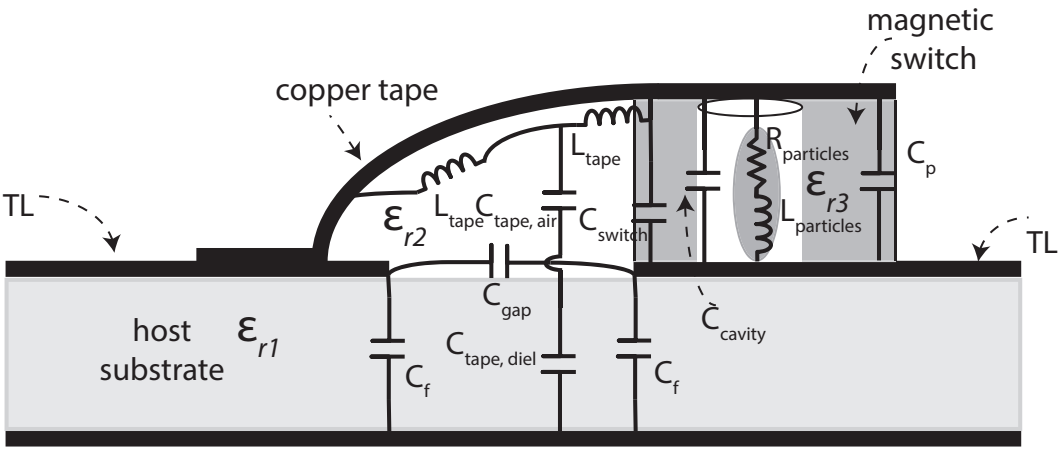

Figure 36. Side View of magnetic switch with proposed equivalent lumped model.

other half of the discontinuous 50-Ω TL. Figure 36 (a) shows the side view of the TL, switch, copper tape, along with the proposed equivalent model of the complete magnetic switch. The capacitance C_f is due to the fringing effect of the opens ends TLs, whereas C_{gap} is the coupling capacitance of the cap. Gap discontinuities are well addressed in microstrip literature and the values of coupling capacitance (C_{gap}) and fringing capacitance C_f were calculated using the formulas given in [31].

The copper tape was considered as a suspended microstrip line of finite length over the air and the host TL substrate (TMM4). This copper tape will have series inductance (L_{tape}) along with the capacitances, $C_{tape,air}$ and $C_{tape,diel}$ because of the suspension in the air and on the TL substrate, respectively. The value of L_{tape} was calculated using the formulas given in [31]. C_{switch} is the a shunt capacitance resulting from the top and bottom copper. C_{cavity} is the shunt capacitance resulting from the top copper tape and bottom conductor, whereas C_p accounts for the effect of open end fringing capacitance of the open end line. The values of C_{tape}, $C_{tape,air}$, $C_{tape,diel}$, C_{switch}, and C_{cavity} were calculated using the formula for parallel plate capacitance, whereas the C_p value was extracted using formula for microstrip discontinuities [31].

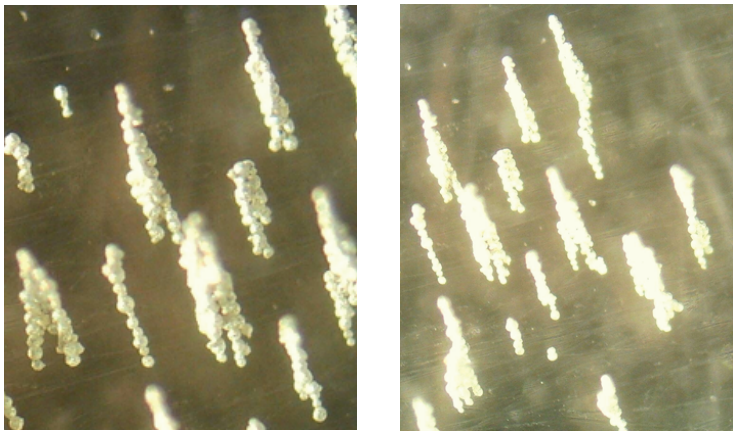

Figure 37. Behavior of magnetic particles in the presence of magnetic field.

$R_{particle}$ was added to model the effect of the magnetic switch in the 'ON' and 'OFF' state in the equivalent circuit. In the switch 'OFF' state the value of $R_{particle}$ will be very high as there will be air in between the top copper tape and bottom conductor, whereas $R_{particles}$ will be a smaller value when the switch will be magnetically activated. The value of $L_{particle}$ was extracted using the theory of microstrip vias, as in the 'ON' state, magnetic particles will build up columns between the top copper tape and the bottom conductor: thus providing a dc current path to the bottom conductor [32], [33]. The formula used for estimating the inductance of the magnetic particles is [33]

$$L_{particle} = \frac{\mu_o}{2\pi}\left[h\ln\left(h\ln\left(\frac{2h+\sqrt{r^2+h^2}}{r}\right)+\frac{3}{2}\left(r-\sqrt{r^2+h^2}\right)\right)\right], \qquad (2.9)$$

where r is the radius of the magnetic particles [26] and h is the height of the substrate. The behavior of the magnetic particles in the presence of magnetic field was observed under a microscope and is shown the Fig. 37. It can be seen from Figure 37 that when a magnet is placed under the sheet containing the particles, particles align in

a column. So, the approach described below can be used to calculate the inductance of the magnetic particles.

As the magnetic switch had 1056 particles in the cavity (one scoop of the measuring cup), the minimum number of magnetic particles per column (N_s) can be estimated using the formula:

$$N_s = \frac{h}{d}, \tag{2.10}$$

where h is the substrate height of the magnetic switch and d is the diameter of the magnetic particles. For substrate height of 0.508 mm (20 mils) and magnetic particle diameter of 0.040 mm (40 micron), the minimum number of magnetic particles per column will be 25. The total number of columns N_C can be well estimated by

$$N_c = \frac{N_T}{N_s} \tag{2.11}$$

where (N_T) is the total number of magnetic particles in the cavity and N_s is the minimum number of magnetic particles per column. For $N_s = 26$ and $N_T = 1056$, the total number columns in 0.508 mm will be approximately 41. In the 'ON' state of the magnetic switch, there will be 41 columns, so there will be 41 paths between the top copper tape and bottom conductor. Therefore, a via will be formed with the 41 columns and will have radius of approx. 0.124 mm. Then, $L_{particle}$ of the magnetic particles in the 'ON' state was calculated using the equation (2.9).

In the absence of the magnetic field ('OFF' state), the magnetic particles will not build up columns in between the top copper tape and bottom conductor. So, in the 'OFF' state these magnetic particles will still form a conducting path between the top layer of magnetic particles and bottom conductor. Therefore, the total particle inductance $L_{particle}$ was calculated using the values 0.254 mm for the height (h) and

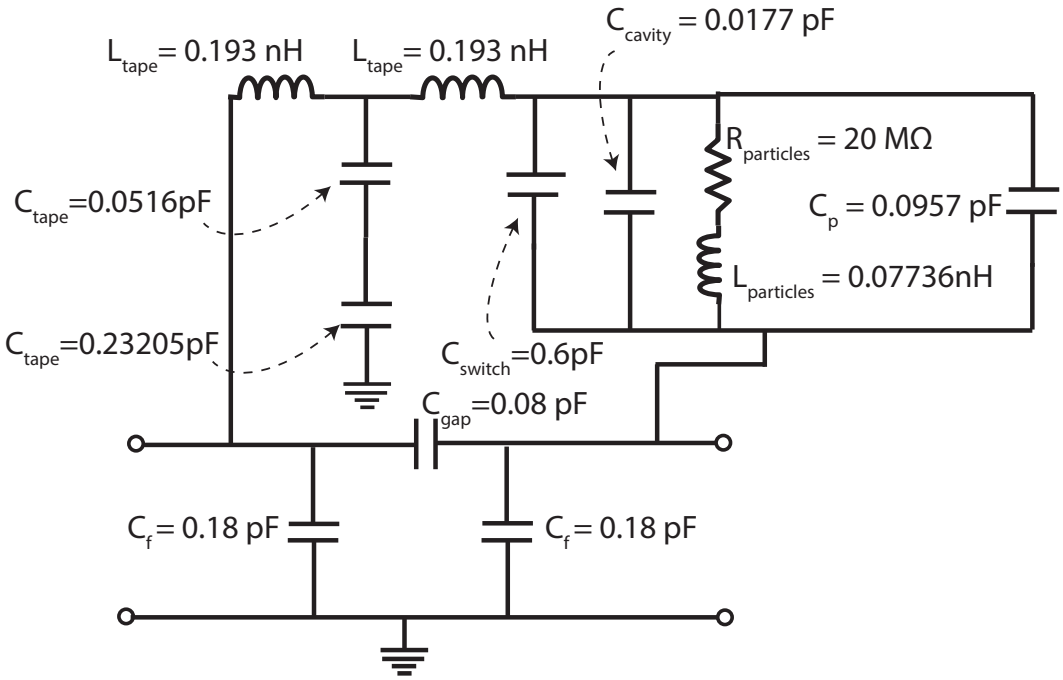

Figure 38. Lumped elements values of the magnetic switch in the 'OFF' state.

0.2 mm for radius (r) in formula (2.9). It was noticed that, because of the high resistance value in the 'OFF' state, the changed value $L_{particle}$ in the 'OFF' state did not contribute significantly in the equivalent model. So, for comparison of the lumped element results with that of results extracted from the ABCD parameters method, the 0.0169 nH value of $L_{particle}$ was used. Figure 38 shows the extracted values of lumped element for the magnetic switch in the 'OFF' state, whereas for the 'ON' state all the extracted values were remain unchanged except for the $R_{particle} = 0.2\ \Omega$.

A comparison between the insertion loss extracted from the circuit model and ABCD conversion (S-parameters) method is shown in the Figure 39. It can be seen from the results that the insertion loss of the proposed magnetic switch is less then 3 dB. Moreover, both the results showed fair agreement, as the lumped model is the approximate equivalent of the magnetic switch and its components. Figure 40 shows the isolation results comparison of the switch in the 'OFF' state. It was shown that

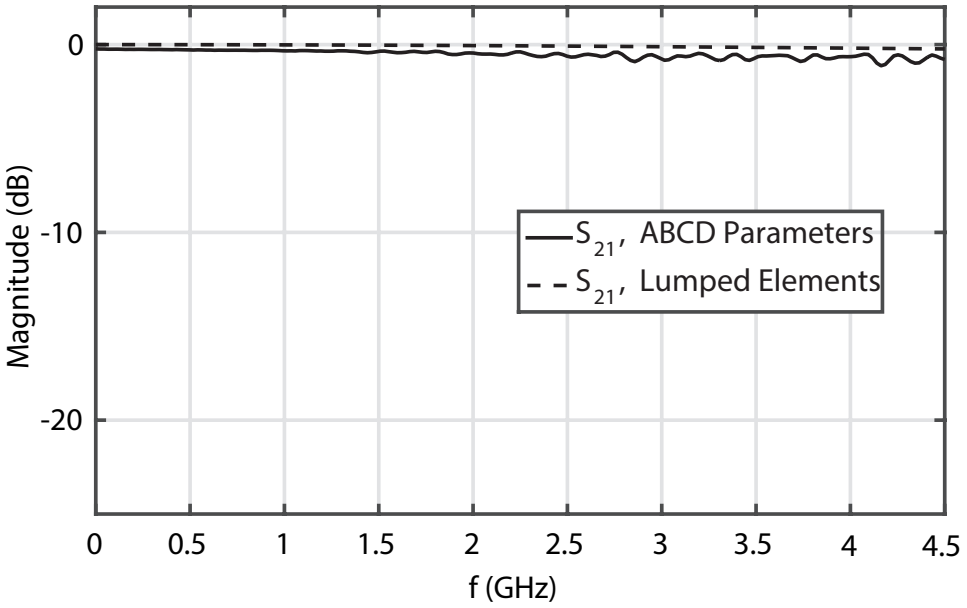

Figure 39. Insertion loss comparison between the circuit model results and ABCD extraction results

the isolation results from the equivalent circuit model are in good agreement with the results extracted from the S-parameter method.

2.7. Conclusions

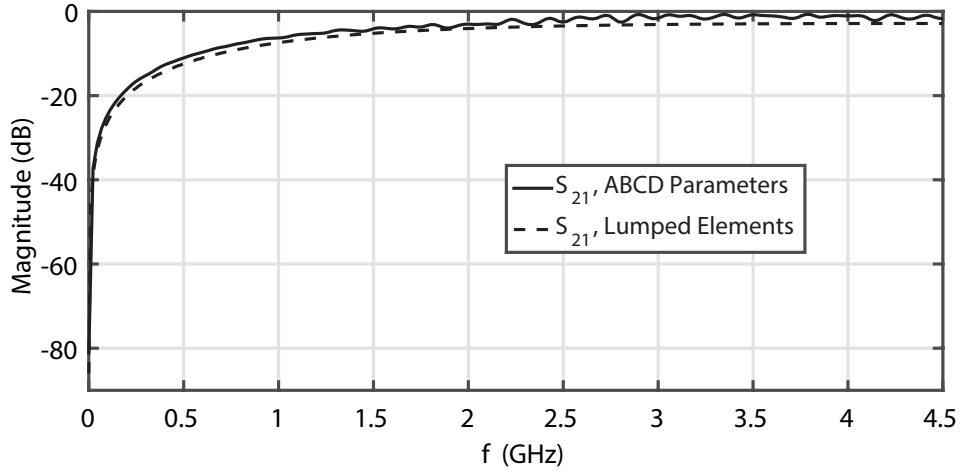

Figure 40. Isolation comparison of the magnetic switch in the 'OFF' state.

In this chapter, a realization, design, and characterization of micro level magnetic switches has been presented. Two micro-level switches: Switch A and Switch B were manufactured and their operational frequency characteristics were further studied along with their behavior in the RF field. Moreover, an approximate lumped element model using the theory of microstrip lines has also been proposed. It can be concluded that both the micro-level switches have good RF switching response. The smaller switch (switch B) has better switching capabilities up to 3 GHz (for a 10 dB isolation threshold), whereas Switch A can only perform switching up to 700 MHz.

CHAPTER 3. RECONFIGURABILITY OF A MICROSTRIP PATCH ANTENNA WITH PARTIALLY FILLED ELECTROMAGNETIC STRUCTURE USING MAGNETIC SWITCHES

3.1. Introduction

A new approach of implementing magnetic switches into printed antennas, that cannot be re-configured using the existing technologies (PIN diodes, RF MEMS, and FETs) is discussed in this chapter. In particular, the design in Figure 41 is proposed here. To understand the reconfigurable mechanism, an equivalent circuit model based on the transmission line theory of the antenna along with the magnetic switch is presented. Furthermore, measurements of the fabricated antenna prototypes

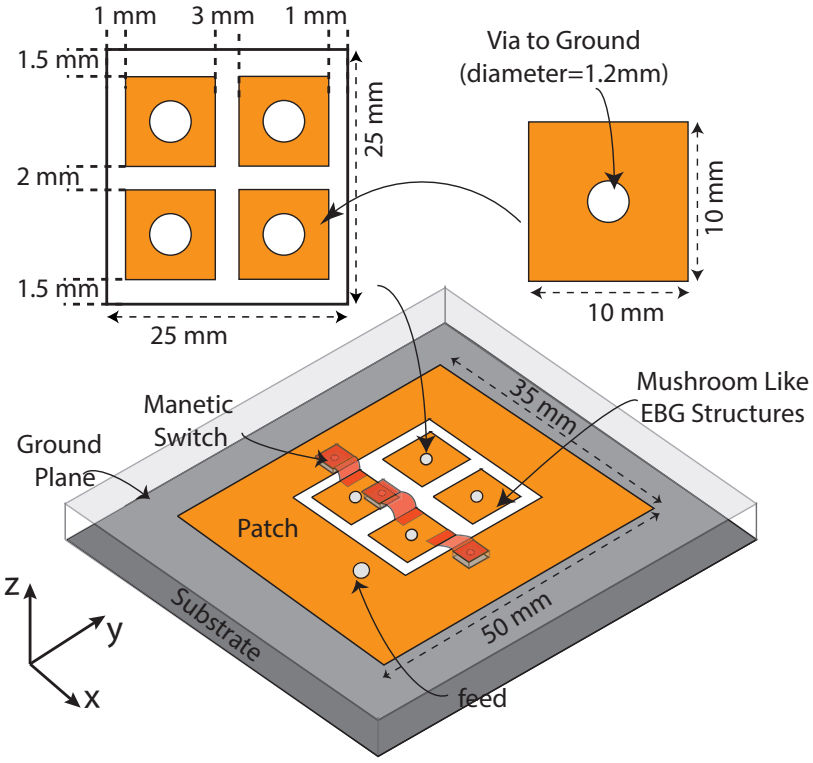

Figure 41. Configuration of the antenna loaded with EBG structure and magnetic switches

are carried out for validation of the return loss. Overall, the simulation and the measurement results of the proposed antenna showed good agreement.

The narrow bandwidth property of the microstrip patch antennas has limited their use in wireless communication systems [34]. For this reason, great efforts have been made in the last decade to achieve low-profile, multiband antennas that can be easily integrated in wireless systems. Some techniques used in the past are multiple layers stacking in the design to achieve multi- frequency responses [35], this approach however increases the physical size of the antenna. Other techniques used in the past are shorting walls [36], stacked patches [37], pairs of slits on the patches [38], and circular arc slots on the printed antennas [39]. A reconfigurable antenna is an alternative to achieve the multiband resonance in the patch antennas. Switching components like PIN diodes, varactor diodes, and RF MEMS switches have normally been used to achieve reconfigurability [40]- [43].

Electromagnetic band gap (EBG) structures have drawn great interest because of their distinctive properties of surface wave suppression, zero phase reflections, altering the electromagnetic interaction between an antenna and the platform, improved antenna performances and antenna size reductions. Furthermore, to achieve the broadband/ multiband characteristics of circularly polarized patch antennas, EBG structures have been used on the bottom of the design, which then increases the overall size of the antenna. Similarly reconfigurability in patch antennas has been achieved by incorporating the switching components between the EBG structures. As EBGs are on the second layer of the design, this provides robustness in the design by increasing the overall size of the antenna. In [44], varactor diodes were used to load the active EBG structure while the CP antenna was on the top of the EBGs thus providing frequency and polarization reconfigurability. This proposed arrangement resulted in an overall size of 171 mm x 171 mm [11]. Steerable antenna arrays with re-configurable

EBG structures is also presented in [45], while a MEMS switch was placed at the root of each fork shaped EBG structure whereas the fork shaped EBG structures were incorporated on the bottom layer of the patch antenna. A reconfigurable beam width antenna using cylindrical EBGs has also been reported in [46], with a radius of 50 mm and having a height of 565 mm. Microstrip patch antennas partially filled with the Metamaterial loaded (EBG) structures on the same layer of the design have been used for the antenna miniaturization in [47]- [48]. However, reconfigurability using these partially filled structures on patch antennas have never been reported in past.

On the other hand, a patch antenna partially filled EBG structure can not be reconfigured in the proposed configuration as shown in the Figure 41. In order to reconfigure the antenna using the PIN diode, there is requirement of the DC biasing circuitry for the PIN diodes which cannot be incorporated in the proposed configuration because of the polarity issues and ground plane connection of the vias in the EBG structure. However, the proposed antenna can be reconfigured in simulation by using a small copper conductor strip between the *Patch* to *EBG*, *EBG* to *EBG*, and *EBG* to *patch* slots. The antenna in the proposed configuration is loaded with the magnetic switches for switching between the slots. As, the magnetic switches do not need any directly connected biasing circuity for their operation, rather they are activated using a small permanent magnet.

3.2. Antenna Configuration and Design Procedure

3.2.1. Reconfigurable Antenna Geometry and Prototyping

The schematic diagram of the proposed reconfigurable antenna is shown in the Figure 41. The proposed design is probe fed having a 2 × 2 mushroom like EBG structure to partially fill the rectangular microstrip patch antenna. The substrate is a Rogers 5880 of permittivity $\epsilon_r = 2.2$, thickness H = 2.54 mm, and loss tangent tanδ = 0.0009. The proposed antenna with the dimensions shown in the Figure 41 and

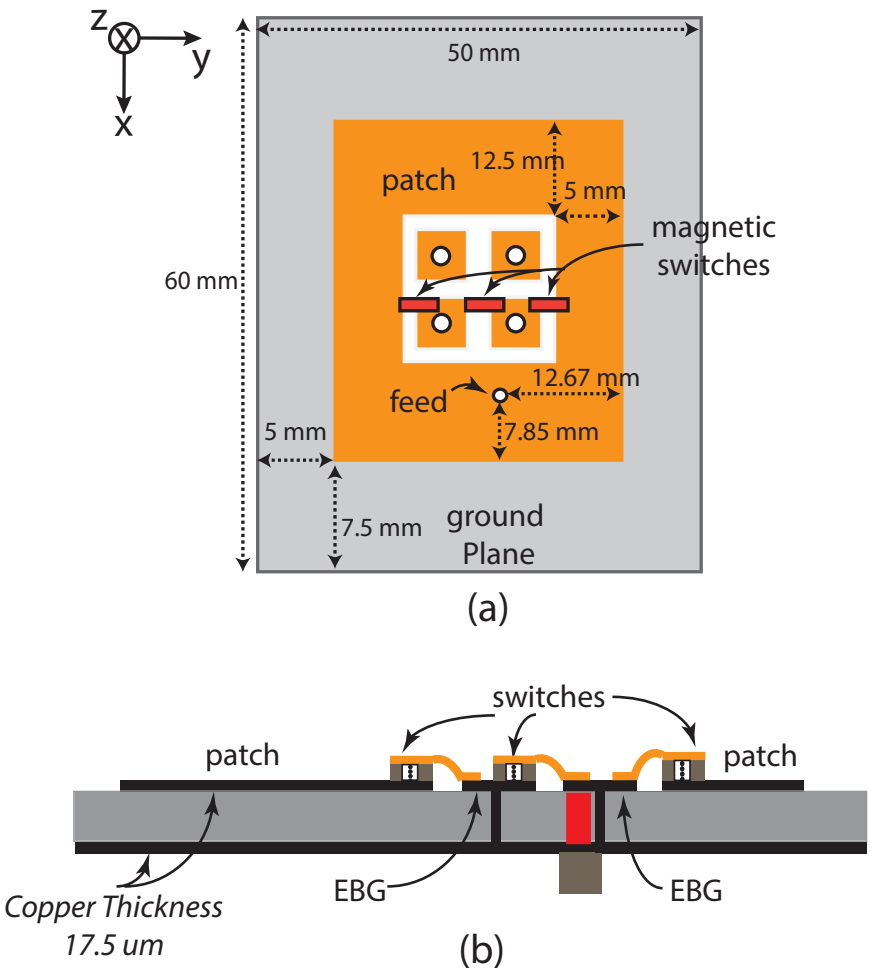

Figure 42. (a). Dimensions of the proposed antenna loaded with EBG structure (top view), (b). Side view of EBG loaded microstrip antenna in switch 'ON' state.

Figure 42 was designed in HFSS (v. 15.0) [24]. The proposed antenna was able to reconfigure to a lower frequency, if a current path is provided between the patch to EBG, EBG to EBG, and then EBG to patch. A small copper conductor was initially used in the simulations to reconfigure the antenna. However, incorporation of the PIN diode or any existing circuitry would require biasing circuity for their operation.

Therefore, this proposed design configuration and layout was not possible to reconfigure using the existing RF switching devices. Three magnetic switches (Switch

B) having a cavity diameter (d) of 0.9 mm, height h = 0.508 mm, and square size of 1.5 mm × 1.5 mm on a TMM4 substrate were used to achieve reconfigurability. As these magnetic switches do not need any biasing circuitry for their operation. The three magnetic switches were modeled with the proposed design in HFSS. A conducting via was used to model the magnetic switch 'ON' state, whereas in the 'OFF' state the via was not included in the simulation. To prove the design concept and working of the magnetic switches to achieve reconfigurability, the proposed design and magnetic switches were fabricated. The cavities are filled with then magnetic particles [26] using the measuring cups (discussed in chapter 2). One scoop of the measuring cup was used to fill each cavity with the magnetic particles. The fabricated antenna with the magnetic switch with copper tape attached to the switches is shown in the Figure 43. The magnetic switches are set 'ON' using a small permanent magnetic on the bottom of the antenna, whereas the 'OFF' state of the magnetic switches were obtained by moving away the permanent magnet.

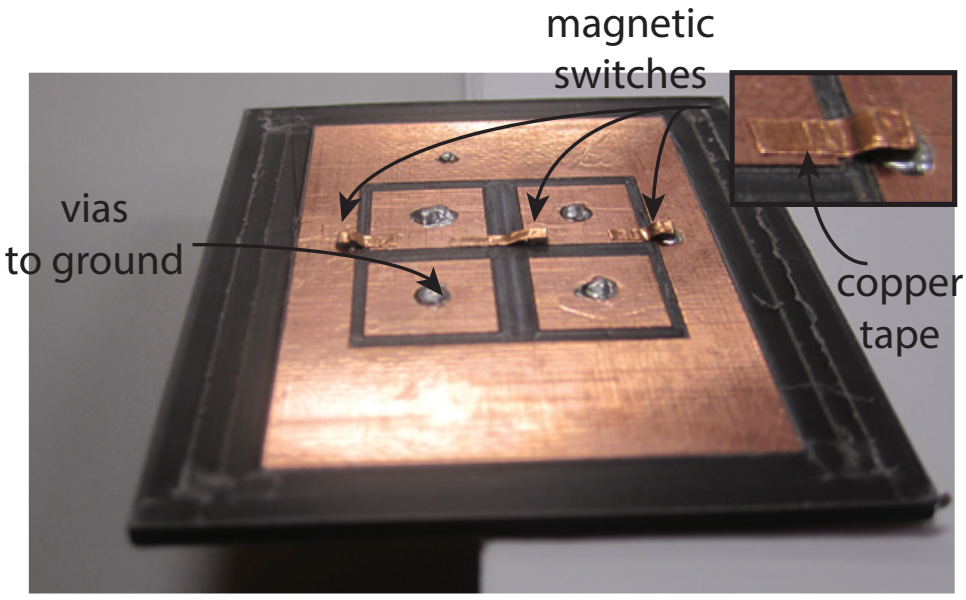

Figure 43. Photograph of the fabricated antenna with the magnetic switches (with particles and copper tape).

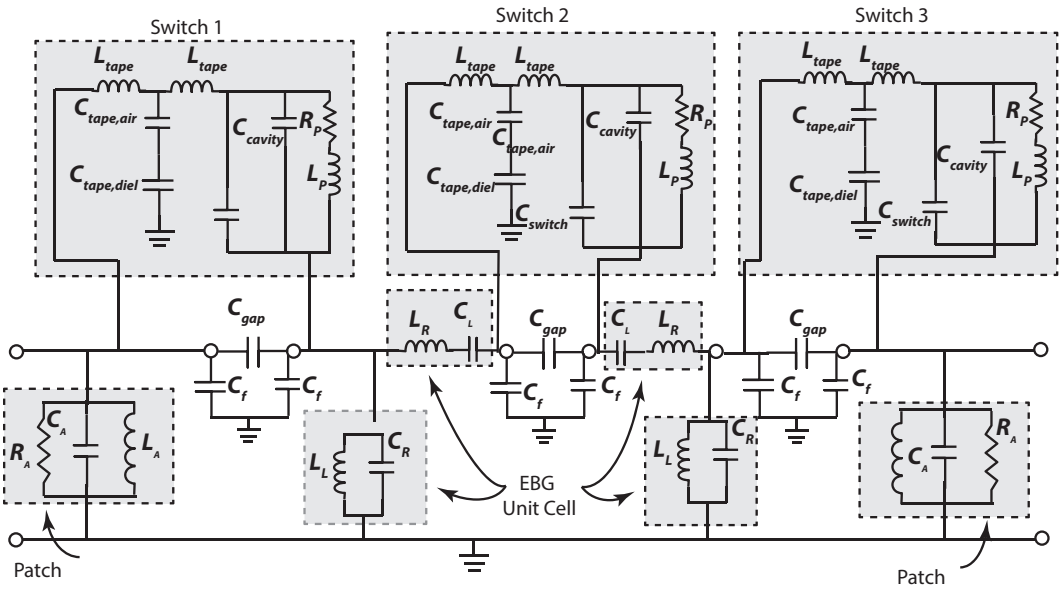

Figure 44. Equivalent circuit model the EBG inspired patch antenna with the magnetic switch model.

3.2.2. Equivalent Circuit Model

The one dimensional circuit representation of the proposed antenna in the biased state of the magnetic switches is described in the Figure 44. The equivalent model is used for the achieving the reconfigurability of the EBG inspired patch antenna. The patch antenna is modeled as a RLC circuit and the EBG structure is modeled using two CRLH unit cells in one dimension [48], which can be observed from Figure 42 (b). As shown in Figure 42 (b), there is a patch antenna on both sides and the two EBG unit cells are present between the patch with a gap of 3.0mm. The patch antenna is modeled as R_A, L_A, and C_A. Magnetic switches are placed between the EBG to Patch antenna EBG to EBG and EBG to patch antenna. C_{gap} and C_f represent the gap capacitance and fringing capacitance, respectively.The L_{tape} and C_{tape} models the inductance and capacitance effect of the copper tape. The capacitance between the top copper and magnetic switch cavity is represented by the C_{switch}, whereas C_{cavity} takes into account of the capacitance because of the cavity. $R_{particles}$ represents the

losses in the switch 'ON' and 'OFF' states. Moreover, $L_{particles}$ accounts for the via inductance because of the magnetic particle columns.

Then, the two EBG structures are modeled as two CRLH unit cells. L_L, C_L represent the left hand inductance and capacitance respectively, while right hand capacitance of the EBG unit cell is represented by C_R and inductance by L_R. When the magnetic switches are in the un-biased states, the equivalent circuit model shown in Figure 44 will remain the same, only the $R_{particle}$ will become very high (because of the air in the cavity). In the un-biased state of the magnetic switch the mushroom like EBG structures will be capacitively coupled to the patch and a high resistance value of $R_{particles}$ will limit the wave to fully pass through the EBG structures; thus providing a lower resonance frequency of 2.21 GHz.

In the presence of the magnetic field, the magnetic switches will be in the 'ON' state and a wave will pass through the EBG to the patch and will be radiated from the radiation resistance R_A of the patch by canceling the inductive and capacitive reactance of the patch antenna. This will increase the overall electrical length of the antenna and cause the resonance of the lower band i.e. 930 MHz.

3.2.3. Current Distribution

The current distribution of the EBG inspired patch antenna was inspected and plotted in Figure 45. It is shown in Figure 45 (a) that in the 'OFF' state the current distribution detours around the slots between the EBG structure and patch antenna, thus the current path becomes shorter. So, current is mainly distributed on the patch only; this makes the electrical length of the antenna shorter. That is why the antenna resonates at a higher frequency in the switch 'OFF' state, whereas in the 'ON' state it passes through the switches and concentrates in the EBG structures and the patch, as shown in Figure 45 (b). This increases the overall electrical length of the proposed structure and makes it resonate at the lower 930 MHz frequency band.

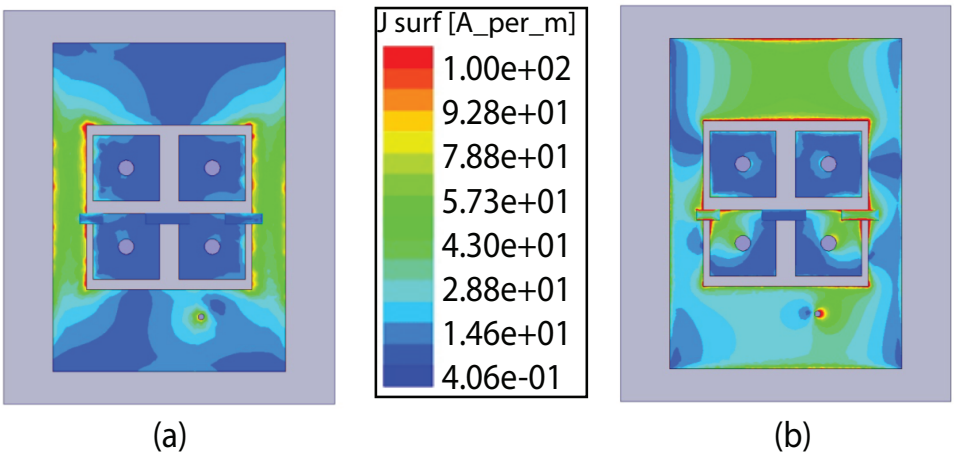

Figure 45. Surface current distribution (a) magnetic switches 'OFF' state and (b) magnetic switches 'ON' state.

3.3. Results and Discussion

The useful switching states, 'OFF-OFF' and 'ON-ON' were provided by the three magnetic switches and used for reconfigurability of the proposed design. HFSS

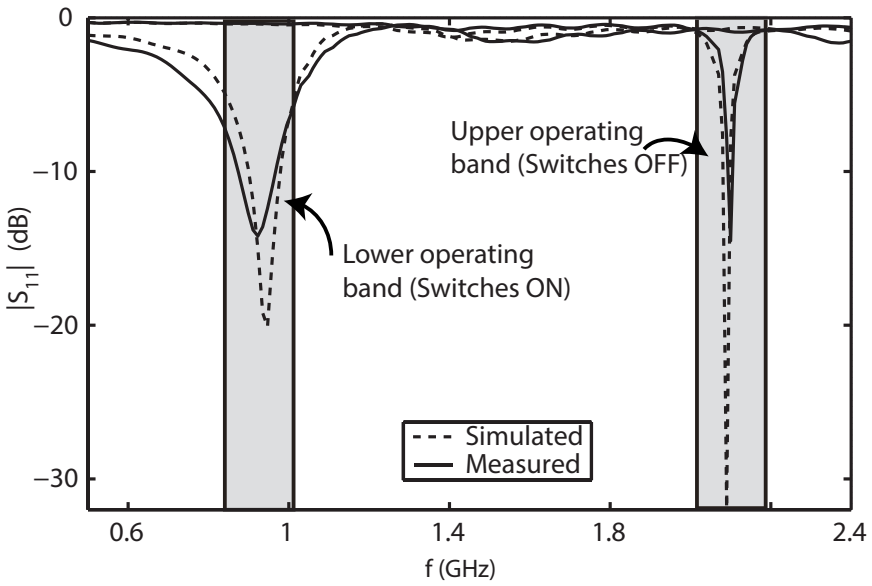

Figure 46. Simulated and measured S-parameters of the reconfigurable EBG inspired patch antenna.

(v 15. 0) [24] was used for the simulation of the proposed design with the magnetic switches and verification, whereas a calibrated Agilent E5071C Vector Network Analyzer (VNA) was used for the measurements of the S-parameters. Figure 46 shows the simulated and measured reflection coefficient magnitudes for the two reconfigured bands. In the absence of the magnetic field (switches 'OFF'), a higher frequency of 2.21 GHz was achieved, whereas the frequency band switched to the lower band in the presence of the magnetic field (switches 'ON').

A novel approach of achieving reconfigurability of the probe fed EBG inspired resonator is presented in this chapter. It was shown that the proposed antenna reconfiguration using existing technologies was not possible. However, the proposed magnetic switches were used in the given layout of the design to achieve frequency switching. The approach showed that any antenna that is hard to reconfigure using existing technologies can be reconfigured using the magnetic switch. The designers can have more freedom to explore the reconfigurable capacity of any antenna.

CHAPTER 4. COMPARISON ANALYSIS OF A FREQUENCY RECONFIGURABLE MICROSTRIP PATCH ANTENNA USING PIN DIODES AND MAGNETIC SWITCHES

4.1. Introduction

In order to increase flexibility of the wireless devices, reconfigurable antennas have been used in wireless devices. The reconfigurability in the antennas have been achieved using PIN Diodes, and other voltage controlled devices such as RF MEMS and varactor diodes. The problem associated with these existing devices is that these devices require DC bias lines for their operation. However, the additional

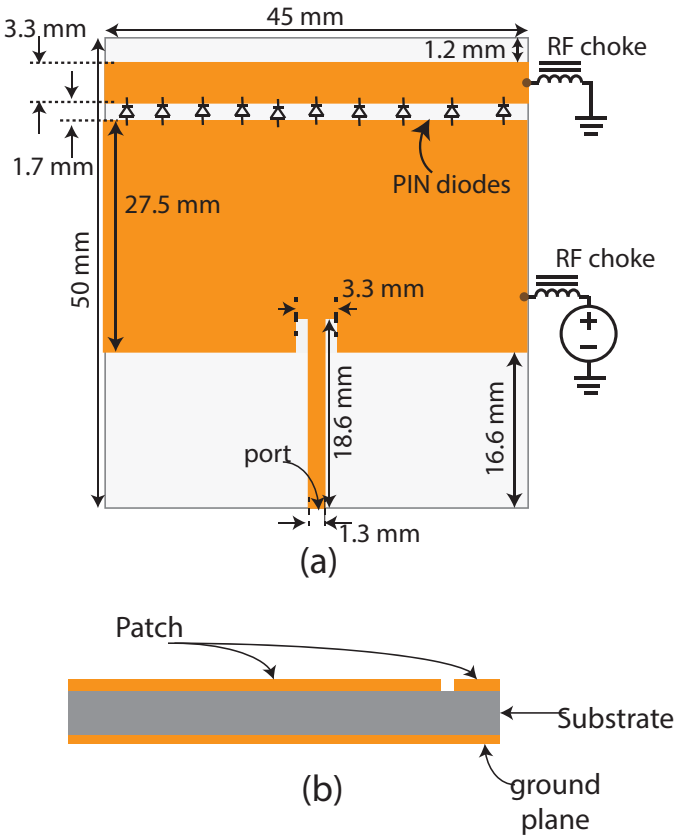

Figure 47. (a). Layout of the prototype reconfigurable patch antenna (top view), (b) side View.

circuitry in the reconfigurable antenna may have an adverse effect on the antenna performance. Moreover, the DC biasing circuitry adds some weight to the existing design. A frequency reconfigurable rectangular microstrip patch antenna using magnetic switches is proposed in this chapter and then the performance analysis of a reconfigured antenna is done by using the PIN diodes in place of the magnetic switches.

4.2. The Reconfigurable Microstrip Patch Antenna using PIN Diodes

For the comparison analysis of the PIN diodes and magnetic switch, a rectangular microstrip antenna in Figure 47 was designed on a TMM4 substrate (relative permittivity 4.5 and loss tangent 0.002) having a thickness of 1.524 mm in HFSS v. 15.0 [24]. The diodes were modeled using the resistance-inductance-capacitance (RLC) boundary sheet in the HFSS. To obtain a good gain and match for the

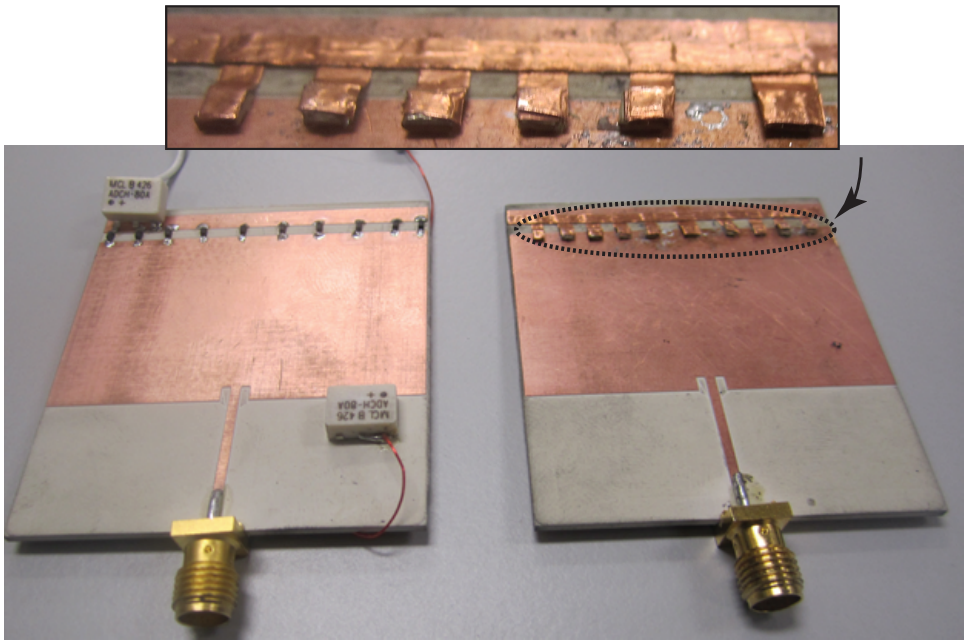

Figure 48. (a). The manufactured reconfigurable patch antenna with PIN Diodes and biasing circuit and (b) fabricated patch antenna with the magnetic switches.

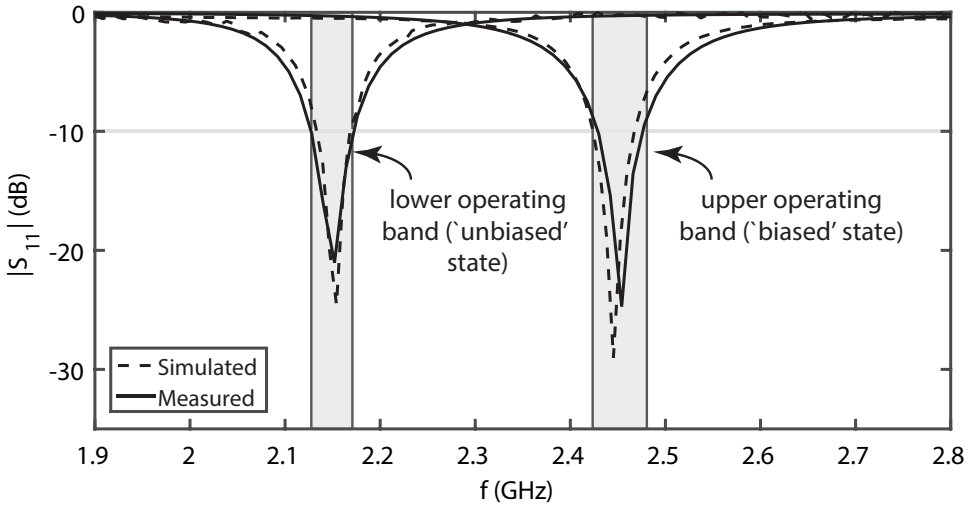

Figure 49. Simulated and measured S-parameters of the reconfigurable patch antenna using PIN diodes.

comparison of the diodes with the magnetic switches, 10 diodes were used for switching between the higher and lower bands. The resistance value of 0.8 Ω and inductance value of 0.5 nH was used in the biased state while in the un-biased state a resistance value of 1.0 kΩ, inductance of 0.5 nH, and capacitance of 0.01 pF were used. The proposed layout of the design has a smaller conducting rectangular strip at a distance of 1.7 mm from the larger rectangular conducting patch. The smaller conducting patch was connected to the main conducting patch using the surface mount controlled PIN diodes. The control voltage was placed on the conducting patch with RF chokes. The PIN diodes were manufactured by Skyworks [49] (SMP 1322), whereas the RF chokes were manufactured by Mini-circuits [50] (ADCH-80A). The manufactured prototype is shown the Figure 48.

The simulation and measurement results of the reflection coefficient ($|S_{11}|$ (dB)) are shown in the Figure 49. When the diodes are not biased, the patch is smaller and resonates at the higher frequency of 2.45 GHz. When the diodes are biased, the patch is much larger and current passes through the diodes to the small conducting strip.

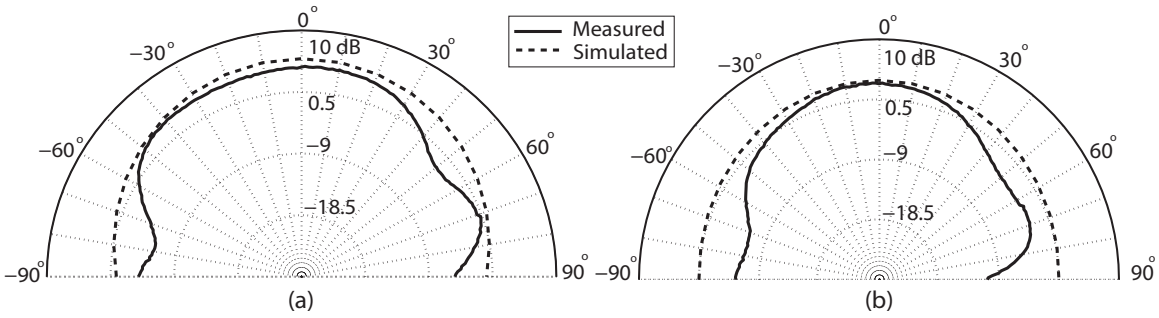

Figure 50. Simulated and measured radiation patterns in the E-plane (xz-plane) for the (a) 'un-biased' state and (b)'biased' state.

So, the antenna resonates at 2.15 GHz. Overall, simulated and measured results of the return loss showed good agreement.

The effect of the PIN diodes on the radiation characteristics of the proposed reconfigurable antenna was investigated by measuring the gain of the patch and radiation pattern. The gain and radiation patterns were measured in an anechoic chamber. The measured gain of the patch antenna was 4.25 dBi when the PIN diodes were unbiased, where as in the diodes biased state the gain dropped down to 2.2 dBi. To demonstrate the radiation characteristics of the reconfigurable patch antenna using

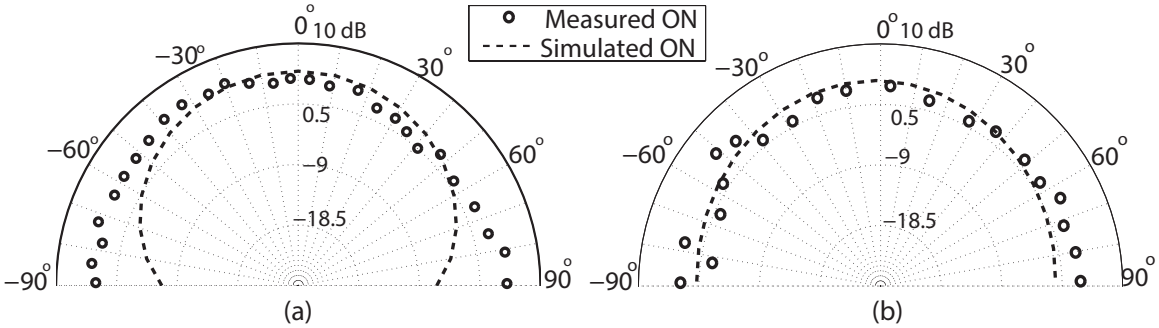

Figure 51. Simulated and measured radiation patterns in the H-plane (yz-plane) for the (a) 'un-biased' state and (b)'biased' state.

PIN diodes, the radiation pattern in the E-plane (xz) and H-plane (yz) are presented in the Figure 50 and Figure 51, respectively. A fairly broadside radiation pattern at both the switching frequencies was obtained except for a null and degraded radiation performance in Figure 50, which is mainly due to the the effect of the incorporated biasing circuitry for the operation of the diodes. Moreover, the gain of the antenna at the lower frequency also decreased from 4.25 dBi to 2.15 dBi.

4.3. Reconfigurability using Magnetic Switches

For the comparison between the PIN diodes and magnetic switches, the reconfigurable antenna shown in the Figure 47 was modeled in the HFSS. The magnetic switch having a cavity diameter 0.45 mm and height 0.508 mm (20 mils) with a square size of 1.5 mm $\times$ 1.5 mm were also modeled in HFSS. To represent the magnetic switches in the 'ON' state in HFSS, a conducting via connecting the bottom of the switch with the top conducting tape was used. Then, when the magnetic switch was in 'OFF' state, the via was removed from the cavity in HFSS, to disconnect the top tape from the bottom plane. The modeled cavities for the magnetic switch were are also fabricated and filled with the magnetic particles. These cavities were attached on the large conducting patch of the antenna using the solder paste. These cavities were then filled with the controlled amount (one scoop of the measuring cup i.e. approx. 1056 particles) of the magnetic particles [26]. The top of the magnetic switch was then connected with the small conducting strip of the rectangular patch antenna using a copper tape. The manufactured prototype with the magnetic switches attached to the antenna is shown in the Figure 48 (b). For a fair comparison of the magnetic switch with the PIN diodes, 10 magnetic switches were attached to the fabricated rectangular patch antenna.

The S-parameters simulation and measurement results are shown in Figure 52. When the magnetic switches were in the 'OFF' state, the patch was smallest and

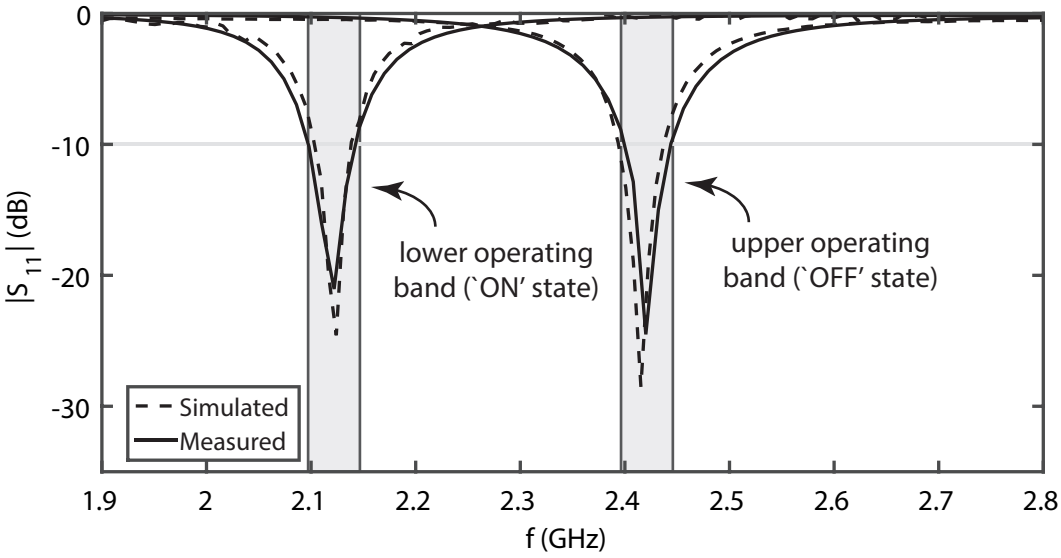

Figure 52. Simulated and measured S-parameters of the reconfigurable antenna using magnetic switches.

resonated at higher frequency band of 2.42 GHz. When the magnetic switches were in the 'ON' state (in the presence of the magnetic field), the electrical length of the patch increased and the antenna operates at a lower frequency band of 2.12 GHz.

To investigate the effect of the magnetic switches on the radiation performance of the reconfigurable antenna, the gain and radiation pattern of the patch antenna

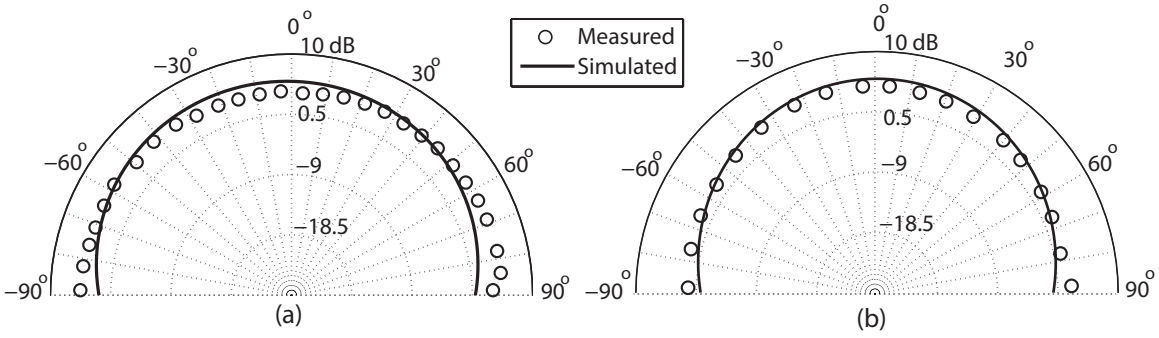

Figure 53. Simulated and measured radiation pattern of the reconfigurable antenna using magnetic switches in the E-plane (x-y) plane (a) 'OFF' state and (b)'ON' state.

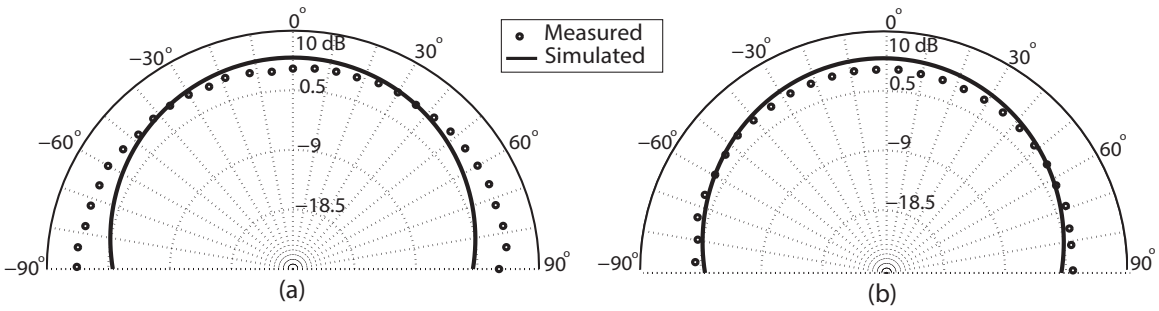

Figure 54. Simulated and measured radiation pattern of the reconfigurable antenna H-plane (yz-plane) (a) 'OFF' state (no magnetic field) and (b)'ON' state (magnetic field).

with magnetic switches in the 'OFF' and 'ON' states was measured in the anechoic chamber. The radiation pattern of the antenna with the magnetic switches in the E-plane (xz-plane) and the H-plane (yz-plane) is shown in Figure 53 and Figure 54, respectively. It can be seen from Figure 53 (a) and Figure 53 (b) that the radiation pattern of the reconfigurable patch antenna is broadside in the switch 'OFF' and 'ON' state. A slight degradation in the the gain of the reconfigurable antenna was observed in the 'ON' state of the switch. The measured gain in the 'OFF' state was 4.3 dBi, whereas in the 'ON' state the gain was 4 dBi. Overall, a good agreement was obtained in the measurements and simulation results.

4.4. Conclusions

The proposed antenna with the 10 PIN diodes and 10 magnetic switches was frequency reconfigured for the comparison and performance analysis of both the RF switches. It was noticed that the PIN diodes incorporation in the design to achieve reconfigurability required a bias line for their operation. These additional circuit components not only added weight to the proposed antenna but also degraded the performance of the antenna in terms of gain and radiation pattern. On the other hand, the magnetic switches were used to reconfigure the same antenna. It is concluded

from the analysis and comparison of the results that magnetic switches do not need any bias lines for their operation, while a permanent magnet that is not the part of the antenna system was used to turn 'OFF' and 'ON' the magnetic switch. So, using magnetic switches, reconfigurable antennas can get rid of the limitations of the housing of additional circuitry on the design.

CHAPTER 5. FURTHER APPLICATIONS OF MAGNETIC SWITCHES

5.1. Introduction

Again, a significant spectrum congestion exists in the wireless field because of the existence of many wireless applications. Thus the design of band reconfigurable antennas help in utilizing the wireless spectrum resources more efficiently. RF switches like PIN diodes, RF MEMS, FETs, and varactor diodes have been used to achieve band reconfigurability. As mentioned before, these exiting RF switches require DC power to switch between a single or multiple bands. A magnetic switch that is proposed in this research can also be a suitable candidate for achieving the frequency switching. To prove the working of the magnetic switch in RF applications, a dipole antenna and a bandpass filter was frequency reconfigured using the magnetic switches and is discussed in this chapter.

5.2. A Reconfigurable Dipole Antenna using Magnetic Switches

Previously, printed dipole antennas have been length-reconfigured with vertical baluns [51]. A printed dipole antenna with integrated via hole balun is designed here

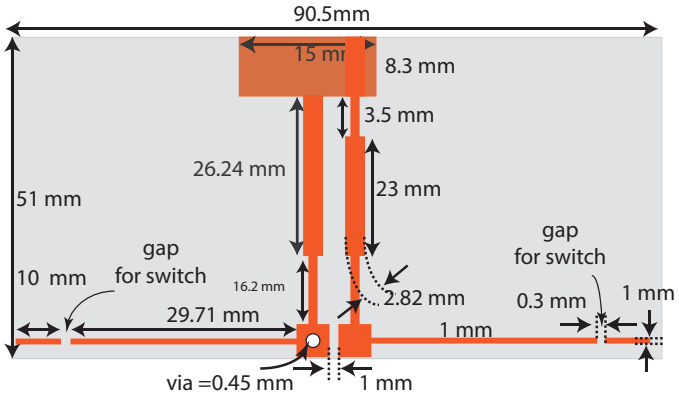

Figure 55. Dimensions of the proposed reconfigurable dipole antenna.

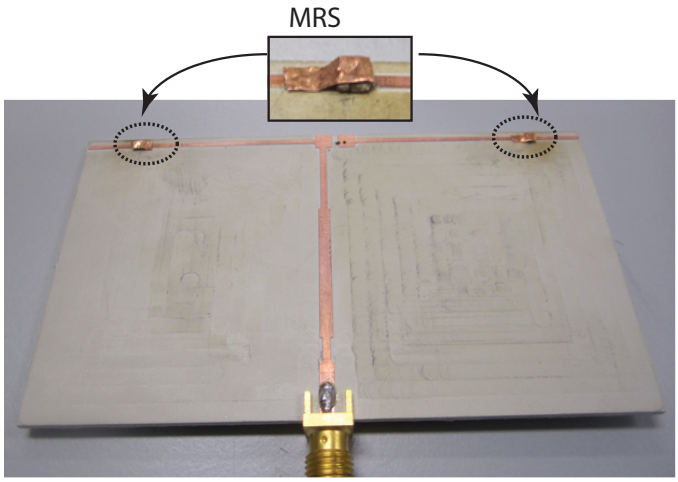

Figure 56. Photograph of the fabricated reconfigurable dipole antenna with magnetic switches.

in HFSS and the printed dipole has two radiating structures having a small strip at a gap of 0.3 mm on both the radiating corners. The design layout and configurations of the printed dipole with the via hole balun is shown in Figure 55. The two arms of the dipole are printed on the top of the TMM4 substrate (thickness 1.524 m,) having a dielectric constant of 4.5. A via hole balun was designed and printed on the bottom of the printed dipole antenna [52]. The balun was designed using the concept of microstrip to strip transition [51] from a 50-Ω to a 70-Ω balanced strip line. The dimensions of the dipole antenna with via hole balun are shown in Figure 55. The thin dipole antenna is reconfigured using magnetic switches between the small gaps. When the magnetic switch is in the 'OFF' state (no magnetic field) the dipole is shorter and the antenna resonates at higher frequency band. When the magnetic switches are in the 'ON' state the antenna length becomes larger and antenna switches to a lower operating band. The manufactured prototype of the reconfigurable antenna with magnetic switches attached to is shown in Figure 56. The magnetic switches had a cavity diameter of 0.45 mm, thickness 0.508 mm, and square size of 1.5 mm $\times$ 1.5 mm.

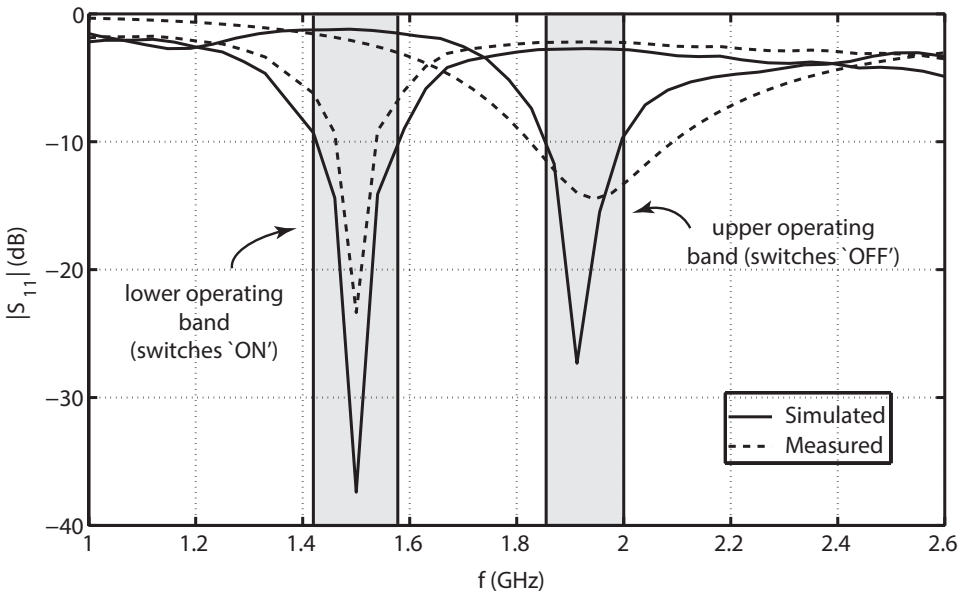

Figure 57. Simulated and measured S-parameters of the reconfigurable dipole antenna.

Figure 57 shows the simulated and measured $|S_{11}|$ (dB) of the reconfigurable dipole antenna with magnetic switches. The simulated lower and upper operating bands are 1.42 GHz to 1.58 GHz and 1.86 GHz to 2 GHz, respectively. Overall, a good agreement results was obtained in the simulations and measurements.

5.3. A Two State Switchable Bandpass Filter using Magnetic Switches

The goal of presenting a bandpass-switchable filter using the proposed magnetic switches in this work is presented next. Designing reconfigurable filters in microwave transducers allow wireless systems to switch between multiple bands using a single filter. PIN diodes and other active devices have been frequently used to achieve discrete state reconfigurability in filters [53]. However, a control signal is always needed for the operation of the active devices to achieve switching between the frequency bands. A reconfigurable bandpass filter using PIN diodes that is able to switch between WIFI and UMTS transmit bands was presented in [54]. Using the design topology and technique discussed in [53], a reconfigurable bandpass filter that

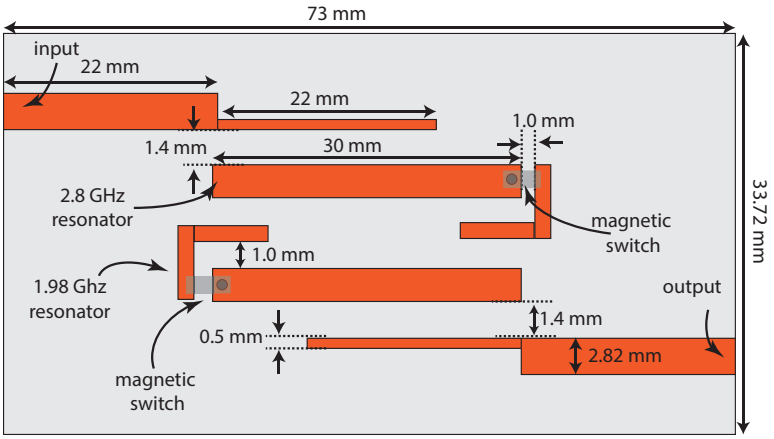

Figure 58. Dimensions of the reconfigurable bandpass filter.

is able to switch between the two bands 2.7 GHz and 1.98 GHz was designed. The design along with the magnetic switches were again modeled in HFSS (v. 15.0) [24]. The dimensions of the proposed reconfigurable filter topology is given in the Figure 58.

The microstrip reconfigurable filter was designed on a TMM4 substrate having a thickness of 1.524 mm ($\epsilon_r = 4.5$ and $\tan\delta = 0.0009$). The center frequency was controlled by adjusting the lengths of the high frequency resonator, where as the bandwidth was controlled by adjusting the capacitive coupling between the high

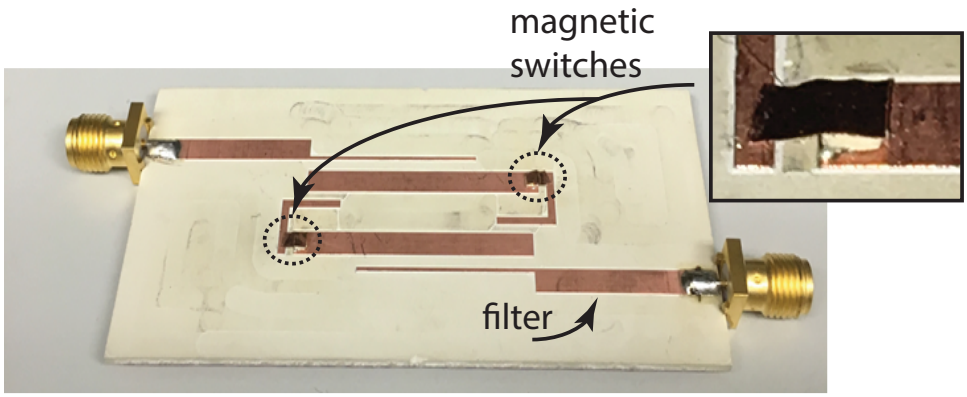

Figure 59. A photograph of the reconfigurable bandpass filter with magnetic switches.

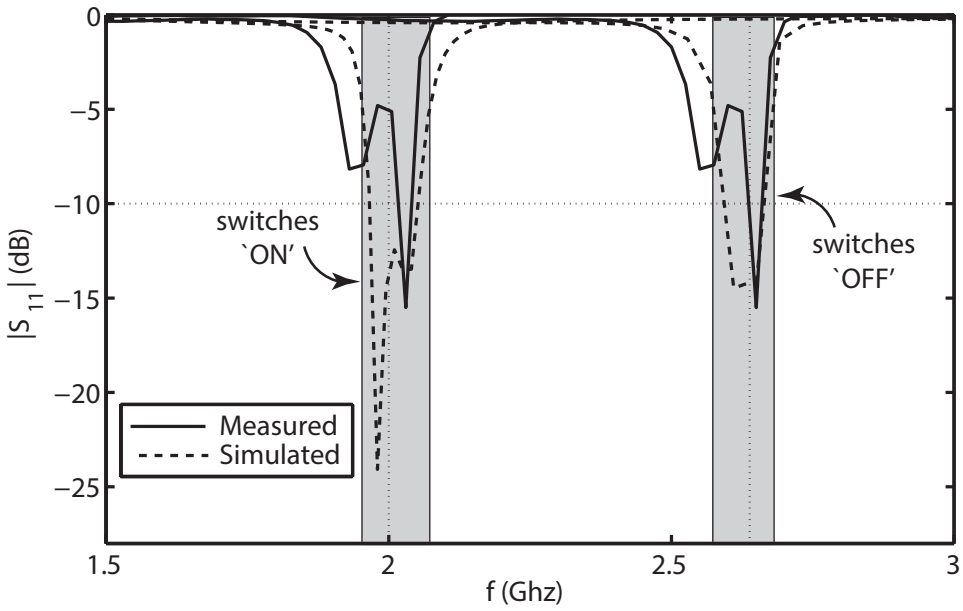

Figure 60. Simulated and measured $|S_{11}|$ (dB) of the reconfigurable bandpass filter in the magnetic switch 'OFF' and 'ON' states.

frequency resonator and folded resonator [54]. A photograph of the fabricated reconfigurable filter with the magnetic switches is shown in the Figure 59. In order to switch between the two frequency bands, magnetic switches were used between the high frequency resonator and folded resonator.

A comparison between the simulated and measured responses of the reconfigurable filter are shown in Figures 60 and 61. The simulated and measured return loss result of the reconfigurable bandpass filter with the magnetic switches in the 'OFF' state (no magnetic field) and the 'ON' state is shown in the Figure 60. It is shown that when the switches are 'OFF' the microstrip strip filter, the return loss at 2.7 GHz pass band is less then 10 dB, whereas in the 'ON' state a good match is observed at 1.98 GHz.

Next, insertion loss (($|S_{21}|$ (dB)) results of the reconfigurable filter with the switch in the 'OFF' state and the 'ON' state are depicted in Figure 61. It can be

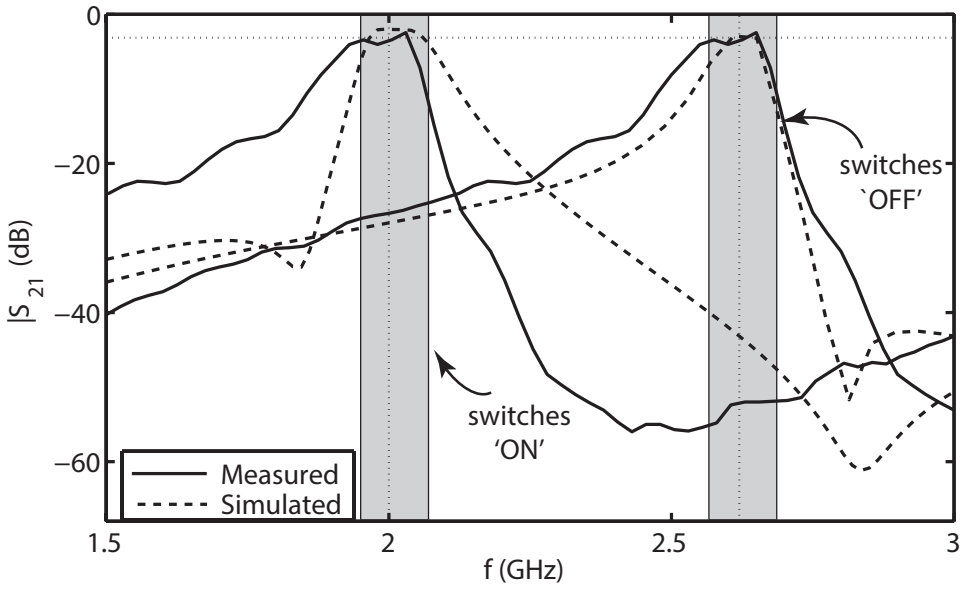

Figure 61. Simulated and measured $|S_{21}|$ (dB) of the reconfigurable bandpass in the magnetic switch 'OFF' and 'ON' states.

seen from Figure 61 that the insertion loss of the filter at 2.69 GHz is around 2.9 dB, while a insertion loss of 2.98 dB was observed in the magnetic switch 'ON' state. A bandwidth of 60 MHz and 50 MHz was obtained in the switches 'OFF' and 'ON' states respectively. Overall, simulated results showed good agreement with the measured results.

5.4. Conclusions

A reconfigurable dipole antenna using magnetic switches and a reconfigurable bandpass filter using the proposed magnetic switches was explained in this chapter. Two states in the length-reconfigurable dipole was achieved using the switches in the 'ON' and 'OFF' states. Similarly, a pass band of 2.7 GHz and 1.98 GHz was achieved using the proposed magnetic switches. It was shown that in order to activate the magnetic switches and activate reconfigurability, no DC bias lines or any other control signaling was added on the printed dipole antenna and bandpass filter prototype.

However, a magnet was used to switch 'ON' the magnetic switch, whereas the 'OFF' state was achieved by moving the magnet away from the fabricated prototypes. Since the magnetic switches that are capable of performing switching up to 3 GHz were modeled, characterized, and explored in this work. It can concluded that below 3 GHz, the magnetic switches can be used for the RF switching in the microwave or antenna system. Thus, the flexibility of using the magnetic switch without adding a control circuitry on the fabricated prototypes revealed that a magnetic switch can also be used as the RF switches.

CHAPTER 6. CONCLUSIONS AND FUTURE WORK

6.1. Conclusions

An initial study of the MEMS based magnetic switch, its implementation, manual manufacturing, and preliminary study of the magnetic switch on discontinuous transmission lines was first discussed. Because of the feasible switching behavior of the magnetic switches in the RF field, micro level magnetic (2nd Gen.) switches using in-house milling capabilities were manufactured. A complete characterization of the micro-level magnetic switches in terms of the S-parameters of the magnetic switch along with the behavior of the magnetic switch was described in this research work. Moreover, an equivalent circuit model and quantification of the magnetic particle was proposed. Good agreement between the S-parameters results and lumped element model was obtained. It is concluded that a micro level magnetic switch (Switch B) having square dimensions of 1.5 mm $\times$ 1.5 mm, cavity diameter 0.45 mm, and height 0.508 mm is capable of switching up to 3 GHz.

Furthermore, to prove the working of the micro level magnetic switches in the antenna systems, a microstrip patch antenna loaded with EBGs that cannot be reconfigured using existing switching technologies was successfully reconfigured using the proposed magnetic switches. It was shown that using proposed magnetic switches in the reconfigurable antenna eliminated the limitation of the DC biasing circuitry. Since the magnetic switches are comprised of particles, which are very light, this made these magnetic switches very useful for the light weight antenna systems. A comparison between the magnetic switches and PIN diodes was also made, and it was shown that PIN diodes degrade the antenna performance as compared to the magnetic switches.

It is concluded that the magnetic switches have the ability to be embedded on the substrate and hence do not need any additional circuit to be installed on

the board to achieve RF switching. Also unlike RF MEMS switches, the proposed magnetic switches do not any expensive packaging to protect movable bridges against the environment. The prototype detail of the magnetic switch from the development and analysis to the application in RF also laid the ground work for future efforts that can include complete industrial packaging of the magnetic switches. Moreover, comparison of the proposed switch with existing technologies and its implementation in antennas prepared a ground work for their implementation in complex antenna systems to achieve reconfigurability. Further micro level switches manufacturing than the proposed switches and achieving switching capability beyond 3 GHz will revolutionize the existing switching techniques and their applications in the antenna systems.

6.2. Recommendations for the Future Work

The work in this research has been concerned with the development, characterization, demonstration, and applications of the proposed magnetic switch in the antenna and microwave systems. A number of open problems must be solved to allow the further development of magnetic switches with switching capabilities beyond 3 GHz. These problems suggest a variety of research directions that can be pursued to allow these magnetic switches to revolutionize existing RF technology. Since these switches require mechanical movement of magnets, one such direction would be to investigate a smarter way to activate magnetic switches without mechanical movement. A direct extension of this work is to explore the switching noise and signal integrity aspects of the magnetic switches. A more professional way to fill the cavity with the magnetic particles can also be explored. A further optimization of the magnetic switches and complete packaging of the proposed switches is also required for their complete working in the industry.

Finally, in terms of applications of the magnetic switches, there is a plethora of possible areas in RF and wireless communication in which these switches can be used, from planar antennas to the complex array systems. Designing phase shifters using magnetic switches and then implementing the phase shifters in self-adapting planar and conformal array systems could be possible future work.

BIBLIOGRAPHY

[1] E. R. Brown, "RF-MEMS Switches for Reconfigurable Integrated Circuits," *IEEE Transactions on MTTs*, Vol. 46, November 1998, pp. 1868-1880.

[2] S. Sharma, M. Gupta, and C.C. Tripathi "Reconfigurable Antennae: A Review", *International Journal of Electronics and Communication Technology*, Vol.2, Issue 3, September 2011.

[3] J. T. Bernhard, R. Wang, R. Clark, and P. Mayes "Stacked Reconfigurable Antenna Elements for Space-based Radar Application", *IEEE AP-S International Symposium,* Vol.1, 2001, pp.158-161.

[4] H. T. Friis, C. B. Feldman, and W. M. Sharpless, "The Determination of the Direction of Arrival of Short Radio Waves", *Proceedings of the Institute of Radio Engineers*, January 1934, pp. 47-78.

[5] D. E. Anagnostou, M. T. Chryssomallis, B. D. Braaten, J. Ebel, and N. Seplveda, "Reconfigurable UWB antenna with RF-MEMS for On-Demand WLAN Rejection", *IEEE Transactions on Antennas and Propagation,* Vol. 62, No. 2, February 2014, pp. 1-7.

[6] J. C. Chiao,Y. Fu, I . M. Chio, M. Delisio, and L. Y. Lin,"MEMS Reconfigurable Vee Antenna", *Microwave Symposium Digest, 1999 IEEE MTT-S International,* Vol. 4, 1999, pp.1515-1518.

[7] F. Yang, and Y. Rahmat-Samii,"A Reconfigurable Patch Antenna Using Switchable Slots for Circular Polarization Diversity", *IEEE Microwave and Wireless Component Letter*, Vol. 12, Issue 3, March 2002, pp.96-98.

[8] J. C. Chiao, Y. Fu, D. Choudhury, and L. Y. Lin, "MEMS Millimeter Wave Components", *IEEE MTT-S International Microwave Symposium Digest, Anaheim, CA* , 1999, pp. 463-466.

[9] D. E. Anagnostou, G. Zheng, M. Chryssomallis, J. Lyke, G. Ponchak, J. Papapolymerou, and C. G. Christodoulou, "Design, Fabrication, and Measurements of an RF-MEMS-Based Self-Similar Reconfigurable Antenna", *IEEE Transactions on Antennas and Propagation, Special Issue on Multifunction Antennas and Antenna Systems,* Vol. 54, Issue 2, Part 1, February 2006, pp. 422-432.

[10] X. Yang, B. Wang, and Y. Zhang, "A Reconfigurable Hilbert Curve Patch Antenna", *IEEE Antennas and Propoagation Society International Symposium,* Vol. 2B, November 1979, pp. 613-616.

[11] G. Huff, J. Feng, D. Zhang, and J. T. Bernard, "A Novel Radiation Pattern and Frequency Reconfigurable Single Turn Square Spiral Microstrip Antenna", *IEEE Microwave and Wireless Component Letters,* Vol. 13, No. 2, January 2003, pp. 57-59.

[12] H. Pan, J. T. Bernhard, and V. K. Nair, "Reconfigurable Single Armed Square Spiral Microstrip Antenna Design", *IEEE International Workshop on Antenna Technology Small Antennas and Novel Metamaterials 2006,* March 2006, pp. 180-183.

[13] G. H. Huff, and J. T. Bernhard "Integration of packaged RF MEMS Switches with Radiation Pattern Reconfigurable Square Spiral Microstrip Antenna", *IEEE Transactions on Antennas and Propagation,* Vol. 54, No. Issue 2, Part 1, February 2006, pp. 464-469.

[14] T. L.Roach, G. H. Huff, and J. T. Bernhard, "On the Applications for Radiation Reconfigurable Antenna", *Second NASA/ESA Conference on Adaptive Hardware and Systems (AHS 2007),* 5-8, August 2007, pp. 7-13.

[15] G. Wang, T. Polley, A. Hunt, and J. Papapolumerou, "A High Performance Tunable RF MEMS Switch Using Barium Stontoum Titanate (BST) Dielectrics for Reconfigurable Antennas and Phassed Arrays ," *IEEE Antennas and Wireless Propagation Letters,* Vol. 4, August 2009, pp. 2242-2251.

[16] F. Yang, Y. R. Samii, "A Reconfigurable Patch Antenna Using Switchable Slote for Circular Polarization Diversity", *IEEE Microwave and Wireless Component Letters,* Vol. 12, No. 3, March 2002.

[17] K. C. Gupta at el., "Design of Frequency Reconfigurable Rectangular Slot Ring Antennas", *IEEE Antenna and Propagation Society International Symposium,* Vol. 1, 2000.

[18] T. Aboufoul, A. Alomainy, and C. Parini, "Reconfigurable UWB Monopole Antenna for Cognitive Radio Applications Using GaAs FET Switches", *IEEE Antennas and Wireless Propagation Letters* Vol. 11, 2012, pp. 392-394.

[19] C. K. Sun, R. Nguyen, C. T. Chang, and D. J. Albare, "Photovoltaic-FET for Optoelectronic RF/μwave Switching", *IEEE Transcations on Microwave Theory and Techniques,* Vol. 44, No. 10, October 1996, pp. 1747-1749.

[20] P. Hindle, "The State of RF/Microwave Switch Devices", *Microwave Journal Editor,* OMRON Electronic Component Press, 2010, Available:https://www.components.omron.com/components/web/webfiles.nsf/press [online].

[21] R. L. Haupt, and M. Lanagan, "Reconfigurable Antennas", *IEEE Antennas and Propagation Magazine,* Vol. 55, No. 1, February 2001, pp. 49-61.

[22] D. Peoulis, K. Sarabandi, and L.P. B. . Latehi,"Design of Reconfigurable Slot Antennas", *IEEE Transactions on Antennas and Propagation,* Vol. 53, No. 2, February 2005, pp. 645-654.

[23] M. F. Ismail, M. K. A. Rahim, and H. A. Majid, "The Investigation of PIN Diode Switch on Reconfigurable Antenna", *2011 IEEE International RF and Microwave Conference,* December 2011, pp. 234-237.

[24] ANSYS HFSS, High Frequency Electromagnetic Field Simulation. Available: www.ansys.com/Products/Electronics/ANSYS-HFSS [online].

[25] Keysight Technologies, Advanced Design System (ADS). Available: www.keysight.com [online].

[26] CONDUCT-O-FIL® Silver-Coated Magnetic Particles. Available: www.pottersbeads.com [online].

[27] W. Y. Hsiang, "On the Sphere Packing Problem and The Proof of Kepler,s Problem Conjecture", *2011 International Journal of Mathematics,* Vol. 4, 1993, pp. 739-830.

[28] David M. Pozar, "Microwave Engineering", 4^{th} Ed., John Wiley & Sons, 2012, pp. 165-227.

[29] Benjamin D Braaten et al., "Fundamental Research on Electromagnetic-Responsive Metamaterials for High Efficient Mobile Cyber-Physical Systems", *Progress for Inter-institutional Collaboration research project entitled,* June 2014.

[30] LPKF, Rapid PCB Prototyping. Available: www.lpkf.com [online].

[31] R. Garg, I. Bahl, M. Bozzi "Microstrip Lines and Slotlines", 3^{rd} Ed., Artech House, 2013.

[32] D. G. Swanson, W. J R. Hoefer, "Microwave Circuit Modeling Using Electromagnetic Field Simulation", Artech House, 2003.

[33] M. E. Goldfrab, R. A. Pucel, "Modeling Via Hole Grounds in Microstrip", *IEEE Microwave and Guided Wave Letters,* Vol. 1, No. 6, June 1991, pp. 135-137.

[34] G. Kumar and K. P. Ray, "Broadband Microstrip Antennas," Boston MA: Arctech House, February 2003, pp. 18-23.

[35] H. F. Abutasrboush, R. Nilavalan, S. W. Cheung, K. M. Nasr, T. Peter, and D. Budimir, "A Reconfigurable Wideband and Multiband Antenna Using Dual Patch Elements For Compact Wireless Devices, *IEEE Trans. on Antennas and Propagation,* Vol. 60, No. 1, January 2012, pp. 36-43.

[36] C. Mak, R. Chair, K. Lee, K. Luk, and A. Kishk, "Half U-slot Patch Antenna With Shortening Wall, *Elect. Lett.,* Vol. 39, 2003, pp. 1779-1780.

[37] J. Anguera, C. Puente, C. Borja, and J. Soler, "Dual-Frequency Broad-band-stacked Microstrip Antenna Using A Reactive Loading And Fractal Shaped Radiating Edge, *IEEE Antennas Propag. Lett.,* Vol. 49, No. 9, 2007, pp. 309-312.

[38] K. L. Wong and W. H. Hsu, "A Broad-band Rectangular Patch With A Pair Wide Slits," *IEEE Trans. Antennas Propag.,* Vol. 49, No. 9, September 2001, pp. 1345-1347.

[39] R. Bhalla and L. Shafai, "Broadband patch Antenna With Circular Arc Shaped Slot," *Proc. IEEE Antennas Propag. Soc. Int. Symp.,* Vol. 1, 2002, pp. 394-397.

[40] A. Sheta and S. Mahmoud, "A Widely Tunable Compact Patch Antenna," *IEEE Antennas Wireless Propag. Lett.,* Vol. 7, 2008, pp. 4042.

[41] A. Mak, C. Rowell, R. Murch, and C. Mak, "Reconfigurable Multiband Antenna Designs For Wireless Communication Devices," *IEEE Trans. Antennas Propag.,* Vol. 55, No. 7, July 2007, pp. 19191928.

[42] S. Yang, C. Zhang, H. Pan, A. Fathy, and V. Nair, "Frequency Re-configurable Antennas For Multiradio Wireless Platforms," *IEEE Microw. Mag.,* Vol. 10, No. 1, February 2009, pp. 6683.

[43] Y. Huang and K. Boyle, "Special Topics" in *Antennas: From Theory to Practice,* John Wiley and Sons Ltd., 2008, pp. 283-356.

[44] B. Liang, B. Sanz-Izquierdo, E. A. Parker, and J. C. Batchelor, "A Frequency and Polarization Reconfigurable Circularly Polarized Antenna Using Active EBG Structure For Satellite Navigation," *IEEE Trans. Antennas Propag.,* Vol. 63, No. 1, January 2015, pp. 33-40.

[45] L. Yang, M. Fan, F. Chen, J. She, and Z. Feng, "A Novel Compact Electromagnetic- bandgap (EBG) Structure And Its Applications For Microwave Circuits," *IEEE Trans. on Microwave Th. and Tech.,* Vol. 53, No. 1, January 2005, pp. 183-190.

[46] A Edalati, and T. A. Denidni, "Reconfigurable Beamwidth Antenna Based On Active Partially Reflective Surfaces," *IEEE Antennas Wireless Propag. Lett.,* Vol. 8, 2009, pp. 1087-1090.

[47] F. Javier, H. Martinez, V. G. Posadas, L. E. G. Munoz, and D. S. Vargas, "Multi-frequency And Dual-mode Patch Antennas Partially Filled With Left-

Handed Structures," *IEEE Trans. Antennas Propag.,* Vol. 56, No. 8, August 2015, pp. 2527-2539.

[48] Y. Dong, H. Toyao, and T. Itoh, "Compact Circularly Polarized Patch Antenna Loaded With Metamaterial Structures," *IEEE Trans. Antennas Propag.,* Vol. 59, No. 11, November 2011, pp. 4329-4333.

[49] Skyworks Inc. Available: www.skyworksinc.com [Online]

[50] Mini-circuits. Available: www.minicircuits.com [Online]

[51] L. Gei and K. Luk, "A Band Reconfigurable Antenna Based On Directed Dipole," *IEEE Trans. on Ant. and Prop.,* Vol. 62, No. 1, January 2014, pp. 64-71.

[52] H. Chuang and L. Kuo "3-D FDTD Design Analysis Of A 2.4 GHz Polarization Diversity Printed Dipole Antenna With Integrated Balun and Polarization Switching Circuit For WLAN and Wireless Communication Application," *IEEE Trans. on Microwave Theory and Techniques,* Vol. 51, No. 2, February 2003, pp. 374 -381.

[53] I. L-. Garro, J. C. Reyes, and Z. B-. Brito, "Recent Advances in Reconfigurable Microwave Filters", *Microwave and Optoelectronics Conference (IMOC), 2011 SBMO/IEEE MTT-S International,* October 2011, pp. 338-346.

[54] Z. B-. Brito, I. L-. Garro, G. N-. Munoz, "UMTS-WIfI Switchable Bandpass Filter", *Proceedings of the 39th European Microwave Conference,* October 2009, pp. 125-128.